Computers and Structures 248 (2021) 106483

Contents lists available at ScienceDirect

Computers and Structures

journal homepage: www.elsevier.com/locate/compstruc

Stochastic dynamic stiffness for damped taut membranes

Xiang Liu [a,b,c,*], Xueyi Zhao [a,b,c], Sondipon Adhikari [d], Xiao Liu [a,b,c]

[a] Key Laboratory of Traffic Safety on Track, Ministry of Education, School of Traffic & Transportation Engineering, Central South University, Changsha, China
[b] Joint International Research Laboratory of Key Technology for Rail Traffic Safety, Central South University, Changsha, China
[c] National & Local Joint Engineering Research Center of Safety Technology for Rail Vehicle, Central South University, Changsha, China
[d] Future Manufacturing Research Institute, College of Engineering, Swansea University, Swansea, UK

ARTICLE INFO

Article history:
Received 12 November 2020
Accepted 13 January 2021
Available online 3 March 2021

Keywords:
Stochastic dynamic stiffness method
Membranes
Stochastic dynamic analysis
KL expansion

ABSTRACT

An analytical stochastic dynamic stiffness formulation is developed for the dynamic analysis of damped membrane structures with parametric uncertainties. First, the exact general solution of a biaxially taut membrane in the frequency domain is derived, which is used as the frequency-dependent shape function. Both the material properties and the tension fields of the membrane are modelled as 2D random fields with an exponential autocorrelation function in both x and y directions. Then, the random fields are decomposed by Karhunen-Loève (KL) expansion. After a formulation procedure like the finite element method, the stochastic stiffness, and mass elemental matrices are derived based on the frequency-dependent shape function and the KL expansion, subsequently forming the stochastic dynamic stiffness matrix. The developed stochastic dynamic stiffness elements can be assembled to model membrane assemblies with general boundary conditions considering uncertainties. The proposed method can be utilized as a feasible technique for the efficient and accurate stochastic dynamic analysis in the whole frequency domain. The current research paves the way for stochastic dynamic stiffness formulation for other two-dimensional structures like plates and shells.

1. Introduction

Uncertainties in complex dynamical systems play a very important role in the dynamic properties. In engineering problems, uncertainties appear not only in the applied loads [1–3] but also in the geometric parameters, material properties [4] and boundary conditions of the model. For distributed parameter systems, parametric uncertainties can be represented by random fields leading to stochastic partial differential equations. Based on the classic analysis, probability theory and statistics, the stochastic mechanics of systems can be determined by quantifying uncertainties in the system parameters. Feasible techniques for predicting the uncertainties in the structural behavior of mechanical systems credibly are receiving considerable attention lately.

Many efforts have been devoted to developing parametric approaches for one-dimensional and two-dimensional structures in computational stochastic mechanics that incorporate uncertainty in classic approaches. In the last several decades, the finite element method in conjunction with perturbation techniques, spectral methods and Monte Carlo simulation (MCS) has been widely investigated by many researchers [5–14], boosting the development of so-called stochastic finite element method (SFEM) and its extensions [15–19]. Besides, Kamiński [20] employed stochastic finite difference method (SFDM) to model the vibration of simply supported square plate. Similar to the SFEM, SFDM also requires fine meshing to represent the original random fields, which increases computational cost. Vilmann and Dasgupta [21] used stochastic boundary element method (SBEM) to develop the fundamental solutions of Mindlin plates with stochastic variation in the thickness. Kaljević and Saigal [22] presented stochastic boundary element formulation for two-dimensional steady-state potential flow through homogeneous domains. Su et al. [23] proposed a stochastic spline fictitious boundary element method for the stochastic vibration analysis of plane elastic problems. Marcin [24] presented the iterative stochastic perturbation-based boundary element method to obtain high-precision probabilistic moments of the structural response. Venini and Mariani [25] developed stochastic Rayleigh–Ritz method for free vibration of orthotropic composite plates. Zhang et al. [26] used multi-domain Rayleigh–Ritz approach together with the generalized polynomial chaos expansion to study the stochastic vibro-acoustic responses. However, the Rayleigh–Ritz method [27] has

* Corresponding author at: Key Laboratory of Traffic Safety on Track, Ministry of Education, School of Traffic & Transportation Engineering, Central South University, Changsha, China.
E-mail addresses: xiangliu06@gmail.com (X. Liu), zxy563675400@csu.edu.cn (X. Zhao), S.Adhikari@swansea.ac.uk (S. Adhikari).

https://doi.org/10.1016/j.compstruc.2021.106483
0045-7949/

difficulty with finding a set of test functions and is limited to regular domains. In combination with a Galerkin method, polynomial chaos expansion is applied to the stochastic analysis of plates in [28,29]. Gupta [30] used a meshless method called element free Galerkin method to solve the elastic buckling of columns. Huang et al. [31–33] used a Fourier-based for the wrinkling of membranes and plates.

Another powerful tool has shown potential in computational stochastic mechanics called dynamic stiffness method (DSM). For deterministic distributed parameter linear dynamical systems, the DSM has been developed to efficiently solve the problem in the frequency domain. In more recent years, the DSM has been applied to the vibration problems of one-dimensional [34,35], two-dimensional structures such as plates and membranes successfully [36–43], their assemblies [44], multibody systems[45] as well as buckling problems [46,40]. In DSM, the shape functions are essentially the exact general solutions derived from the frequency-dependent governing differential equations. This is superior to both the conventional FEM and BEM whose shape functions are approximate and are generally applicable to the low-frequency range. Therefore, exact solutions can be obtained from the DSM without mesh refinement as in the FEM and FDM. As a result, the DSM is computationally efficient for the whole frequency ranges, which is overwhelmingly superior to the element based methods like the FEM and BEM, especially within the medium and high frequency. Some researchers have performed seminal researches to extend the DSM to the stochastic analysis. Inspired by the aforementioned SFEM where the random fields are described by the spectral method [9,10,47,48], Adhikari [49] derived frequency-dependent stochastic dynamic stiffness matrix for axial and bending vibration of rods by using doubly spectral techniques (one for the random fields and the other for the dynamic displacement fields). However, no attempt has been made on stochastic dynamic stiffness method for two-dimensional structures.

In this paper, we focus our attention on two-dimensional structural dynamic analysis with parametric uncertainties and develop the stochastic dynamic stiffness formulation for the damped vibration of membrane structures. For the eigenvalue analysis, the material property and tensions are assumed to be Gaussian random variables. Through the Monte Carlo simulation to generate samples for the random variables, the natural frequencies of an undamped membrane can be directly obtained from the DSM. While for the dynamic response analysis, by considering random fields with exponential autocorrelation functions for both x and y directions, the material property and the pretensions of the membrane are characterized by a set of random fields and represented by Karhunen–Loéve (KL) expansion in each direction. Based on the exact shape function derived from the deterministic damped membrane, the frequency-dependent stochastic element stiffness and mass matrices for a damped membrane element are formulated by incorporating the spectral expansion of the random fields. Subsequently, a stochastic dynamic stiffness matrix is developed for a membrane element with uncertainties. A membrane assembly consisting of elements with different means and variations of material properties and prestresses can therefore be modelled easily following an assembly procedure. The modal analysis and dynamic response analysis of such a membrane assembly can be performed for a wide frequency range by using associated solution techniques. In particular for dynamic response analysis, a superposition technique is used to facilitate the response analysis subjected to any form of excitations such as uniform loads, concentrated loads and non-uniform loads. Essentially, this work presents major contributions to derive analytical formulations for stochastic analysis of the membrane structures within a wide frequency range by combining the merits of both the KL spectral expansion and DSM mentioned above. The proposed method also provides a feasible technique for efficient and accurate stochastic analysis of other two-dimensional structures like plates and shells.

This paper is organized as follows. Section 2 presents the general theory of the KL expansion and its application in stochastic dynamic stiffness method. In Section 3, the deterministic dynamic stiffness formulations for membranes are briefly recalled. In Section 4, the elemental stochastic mass and stiffness matrices are derived to obtain the stochastic dynamic stiffness matrix by using the stochastic dynamic stiffness method. In Section 5, the basic theory of stochastic dynamic response analysis for two-dimensional structures is described. In Section 6, numerical results of the developed formulation are obtained by Monte-Carlo simulation. The conclusions are discussed in the last section.

2. General theory for stochastic dynamic stiffness method for structures by using KL expansion

Problems of structural dynamics in which the uncertainty in specifying stiffness and mass of the structure is modelled within the framework of random fields can be treated using the stochastic finite element method [50,51]. The application of the stochastic finite element method to linear structural dynamics problems typically consists of the following key steps:

1. Selection of appropriate probabilistic models for parameter uncertainties and boundary conditions.
2. Replacement of the element property random fields by an equivalent set of a finite number of random variables. This step, known as the 'discretisation of random fields' is a major step in the analysis.
3. Formulation of the system equations of motion of the form $\mathbf{D}(\omega)\mathbf{u} = \mathbf{f}$ where $\mathbf{D}(\omega)$ is the stochastic dynamic stiffness matrix, $\mathbf{u}$ is the vector of random nodal displacement, and $\mathbf{f}$ is the vector of applied forces. In general, $\mathbf{D}(\omega)$ is a random symmetric complex matrix.
4. Solution of the set of the complex random algebraic equation to obtain the statistics of the response vectors. Alternatively, the response statistics can also be obtained by solving the underlying random eigenvalue problem (see, for example, [52–54] and references therein).

We consider $(\Theta, \mathscr{F}, P)$ be a probability space with $\theta \in \Theta$ denoting a sampling point in the sampling space Θ, $\mathscr{F}$ is the complete σ-algebra over the subsets of Θ and P is the probability measure. Suppose the spatial coordinate vector $\mathbf{r} \in \mathbb{R}^d$ where $d \in \mathscr{I} \leqslant 3$ is the spatial dimension of the problem. Consider $H : (\mathbb{R}^d \times \Theta) \to \mathbb{R}$ is a random field with a covariance function $C_H : (\mathbb{R}^d \times \mathbb{R}^d) \to \mathbb{R}$ defined in a space $\mathscr{D} \in \mathbb{R}^d$. Since the covariance function is finite, symmetric and positive definite it can be represented by a spectral decomposition. Using this spectral decomposition, the random process $H(\mathbf{r}, \theta)$ can be expressed in a generalized Fourier type of series as

$$H(\mathbf{r}, \theta) = H_0(\mathbf{r}) + \sum_{j=1}^{\infty} \sqrt{\lambda_j}\xi_j(\theta)\varphi_j(\mathbf{r}) \tag{1}$$

where $\xi_j(\theta)$ are uncorrelated random variables, λ_j and $\varphi_j(\mathbf{r})$ are eigenvalues and eigenfunctions satisfying the integral equation

$$\int_{\mathscr{D}} C_H(\mathbf{r}_1, \mathbf{r}_2)\varphi_j(\mathbf{r}_1)\mathrm{d}\mathbf{r}_1 = \lambda_j\varphi_j(\mathbf{r}_2), \quad \forall j = 1, 2, \cdots \tag{2}$$

These associated eigenvalues and eigenfunctions will be used to obtain the element mass, stiffness and damping matrices. We refer the books by [50,55] and few recent references [56–58] for further

discussions on Karhunen-Loève expansion. In fact, there are many kinds of correlation function models of random fields, for example, exponential type and squared exponential type. Gaussian random fields with exponentially decaying autocorrelation function are considered in this paper. For all practical purposes, the series in Eq. (1) can be ordered in a decreasing one so that it can be truncated using a finite number of terms with the desired accuracy. The number of terms could be selected based on the 'amount of information' to be retained. The terms mainly depend on the correlation length of the underlying random field. One needs more terms when the correlation length is small.

A linear damped distributed parameter dynamical system in which the displacement variable $U(\mathbf{r},t)$, where $\mathbf{r}\in\mathbb{R}^d$ is the spatial position vector, $d\leqslant 3$ is the dimension of the model and t is time, specified in some domain $\mathscr{D}$, is governed by a linear partial differential equation (see for example [59]):

$$\rho(\mathbf{r},\theta)\frac{\partial^2 U(\mathbf{r},t)}{\partial t^2}+L_1(\theta)\frac{\partial U(\mathbf{r},t)}{\partial t}+L_2(\theta)U(\mathbf{r},t)=p(\mathbf{r},t);\quad \mathbf{r}\in\mathscr{D},t\in T \tag{3}$$

with linear boundary-initial conditions of the form

$$M_{1j}\frac{\partial U(\mathbf{r},t)}{\partial t}=0;\quad M_{2j}U(\mathbf{r},t)=0;\quad \mathbf{r}\in\partial\mathscr{D},\ t=t_0,\ j=1,2,\cdots \tag{4}$$

specified on some boundary surface $\partial\mathscr{D}$. In the above equation, $T\in\mathbb{R}$ is the domain of the time variable t, $\rho(\mathbf{r},\theta)$ is the random mass distribution of the system, $p(\mathbf{r},t)$ is the distributed time-varying forcing function, L_1 is the random spatial self-adjoint damping operator, L_2 is the random spatial self-adjoint stiffness operator and M_{1j} and M_{2j} are some linear operators defined on the boundary surface $\partial\mathscr{D}$. When parametric uncertainties are considered, the mass density $\rho(\mathbf{r},\theta):(\mathbb{R}^d\times\Theta)\to\mathbb{R}$ as well as the damping and stiffness operators involve random processes. Frequency dependent random element stiffness matrices were derived by various authors using the dynamic weighted integral approach [60–63], the energy operator approach [64], sub-structure approach [65] and a series expansion approach [66]. While numerical methods were used in these studies, in this paper exact closed-from analytical expressions will be derived for the element matrices. Below we briefly summarise the derivations in references [49,67], which is adopted in this paper.

Suppose the underlying deterministic homogeneous system corresponding to Eq. (3) without any forcing (see for example [59]) is given by

$$\rho_0\frac{\partial^2 U(\mathbf{r},t)}{\partial t^2}+L_{10}\frac{\partial U(\mathbf{r},t)}{\partial t}+L_{20}U(\mathbf{r},t)=0;\quad \mathbf{r}\in\mathscr{D} \tag{5}$$

Taking the Fourier transform of Eq. (5) one has

$$-\omega^2\rho_0 u(\mathbf{r},\omega)+\mathrm{i}\omega L_{10}\{u(\mathbf{r},\omega)\}+L_{20}\{u(\mathbf{r},\omega)\}=0 \tag{6}$$

where $\omega\in[0,\Omega]$ is the frequency and $\Omega\in\mathbb{R}$ denotes the maximum frequency.

Suppose that frequency-dependent displacement within an element is interpolated from the nodal displacements as

$$u_e(\mathbf{r},\omega)=\mathbf{N}^T(\mathbf{r},\omega)\widehat{\mathbf{u}}_e(\omega) \tag{7}$$

where

$$\mathbf{N}(\mathbf{r},\omega)=\mathbf{\Gamma}(\omega)\mathbf{s}(\mathbf{r},\omega) \tag{8}$$

Here $\widehat{\mathbf{u}}_e(\omega)\in\mathbb{C}^n$ is the nodal displacement vector and $\mathbf{N}(\mathbf{r},\omega)\in\mathbb{C}^n$, the vector of frequency-dependent shape functions and n is the number of the nodal degrees-of-freedom. The vector $\mathbf{s}(\mathbf{r},\omega)=\{s_j(\mathbf{r},\omega)\}^T,\forall j=1,2,\cdots m$ and the $s_j(\mathbf{r},\omega)\in\mathbb{C}$ are the basis functions which exactly satisfy Eq. (6). Here m is the order of the differential equation. The complex matrix $\mathbf{\Gamma}(\omega)\in\mathbb{C}^{n\times m}$ depends on the boundary conditions.

Extending the weak-form of finite element approach to the complex domain, the frequency dependent $n\times n$ complex random stiffness, mass and damping matrices can be obtained as

$$\mathbf{K}_e(\omega,\theta)=\int_{\mathscr{D}_e}k_s(\mathbf{r},\theta)\mathscr{L}_2\{\mathbf{N}(\mathbf{r},\omega)\}\mathscr{L}_2\left\{\mathbf{N}^T(\mathbf{r},\omega)\right\}\mathrm{d}\mathbf{r} \tag{9}$$

$$\mathbf{M}_e(\omega,\theta)=\int_{\mathscr{D}_e}\rho(\mathbf{r},\theta)\mathbf{N}(\mathbf{r},\omega)\mathbf{N}^T(\mathbf{r},\omega)\mathrm{d}\mathbf{r}\quad\text{and} \tag{10}$$

$$\mathbf{C}_e(\omega,\theta)=\int_{\mathscr{D}_e}c(\mathbf{r},\theta)\mathscr{L}_1\{\mathbf{N}(\mathbf{r},\omega)\}\mathscr{L}_1\left\{\mathbf{N}^T(\mathbf{r},\omega)\right\}\mathrm{d}\mathbf{r} \tag{11}$$

where $(\bullet)^T$ denotes matrix transpose, $k_s(\mathbf{r},\theta):(\mathbb{R}^d\times\Theta)\to\mathbb{R}$ is the random distributed stiffness parameter, $\mathscr{L}_2\{\bullet\}$ is the strain energy operator, $c(\mathbf{r},\theta):(\mathbb{R}^d\times\Theta)\to\mathbb{R}$ is the random distributed damping parameter and $\mathscr{L}_1\{\bullet\}$ is the energy dissipation operator. The random fields $k_s(\mathbf{r},\theta),\rho(\mathbf{r},\theta)$ and $c(\mathbf{r},\theta)$ are expanded using the Karhunen-Loève expansion of Eq. (1). Using finite number of terms, each of the complex element matrices can be expanded in a spectral series as

$$\mathbf{K}_e(\omega,\theta)=\mathbf{K}_{0e}(\omega)+\sum_{j=1}^{M_\mathrm{K}}\xi_{\mathrm{K}_j}(\theta)\mathbf{K}_{je}(\omega) \tag{12}$$

$$\mathbf{M}_e(\omega,\theta)=\mathbf{M}_{0e}(\omega)+\sum_{j=1}^{M_\mathrm{M}}\xi_{\mathrm{M}_j}(\theta)\mathbf{M}_{je}(\omega) \tag{13}$$

$$\text{and}\quad \mathbf{C}_e(\omega,\theta)=\mathbf{C}_{0e}(\omega)+\sum_{j=1}^{M_\mathrm{C}}\xi_{\mathrm{C}_j}(\theta)\mathbf{C}_{je}(\omega) \tag{14}$$

Here the complex deterministic symmetric matrices, for example in the case of the stiffness matrix, can be obtained as

$$\mathbf{K}_{0e}(\omega)=\int_{\mathscr{D}_e}k_{s_0}(\mathbf{r})\mathscr{L}_2\{\mathbf{N}(\mathbf{r},\omega)\}\mathscr{L}_2\left\{\mathbf{N}^T(\mathbf{r},\omega)\right\}\mathrm{d}\mathbf{r}\quad\text{and} \tag{15}$$

$$\mathbf{K}_{je}(\omega)=\sqrt{\lambda_{\mathrm{K}_j}}\int_{\mathscr{D}_e}\varphi_{\mathrm{K}_j}(\mathbf{r})\mathscr{L}_2\{\mathbf{N}(\mathbf{r},\omega)\}\mathscr{L}_2\left\{\mathbf{N}^T(\mathbf{r},\omega)\right\}\mathrm{d}\mathbf{r} \tag{16}$$

$\forall j=1,2,\cdots,M_\mathrm{K}$

The equivalent terms corresponding to the mass and damping matrices can also be obtained in a similar manner. Substituting the shape function from Eq. (8), into Eqs. (15) and (16) one obtains

$$\mathbf{K}_{0e}(\omega)=\mathbf{\Gamma}(\omega)\widetilde{\mathbf{K}}_{0e}(\omega)\mathbf{\Gamma}^T(\omega)\quad\text{and} \tag{17}$$

$$\mathbf{K}_{je}(\omega)=\sqrt{\lambda_{\mathrm{K}_j}}\mathbf{\Gamma}(\omega)\widetilde{\mathbf{K}}_{je}(\omega)\mathbf{\Gamma}^T(\omega);\quad\forall j=1,2,\cdots,M_\mathrm{K} \tag{18}$$

where

$$\widetilde{\mathbf{K}}_{0e}(\omega)=\int_{\mathscr{D}_e}k_{s_0}(\mathbf{r})\mathscr{L}_2\{\mathbf{s}(\mathbf{r},\omega)\}\mathscr{L}_2\{\mathbf{s}^T(\mathbf{r},\omega)\}\mathrm{d}\mathbf{r}\in\mathbb{C}^{N\times N}\quad\text{and} \tag{19}$$

$$\widetilde{\mathbf{K}}_{je}(\omega)=\int_{\mathscr{D}_e}\varphi_{\mathrm{K}_j}(\mathbf{r})\mathscr{L}_2\{\mathbf{s}(\mathbf{r},\omega)\}\mathscr{L}_2\{\mathbf{s}^T(\mathbf{r},\omega)\}\mathrm{d}\mathbf{r}\in\mathbb{C}^{N\times N} \tag{20}$$
$$\forall j=1,2,\cdots,M_\mathrm{K}$$

Once the element stiffness, mass and damping matrices are obtained in this manner, the global matrices can be calculated by summing the element matrices with suitable coordinate transformations as in the standard finite element method. A closed-form expression of the eigenfunctions appearing in Eq. (20) are available for only few specific correlation functions and with simple boundaries only. For such cases, as will be seen later in the paper, the integral in Eq. (20) may be obtained in closed-form.

Due to the use of spectral element in the frequency domain, only one finite element is required per physical 'element' of a built-up system. For this reason, the dimension of the global assembled matrices become small even when high-frequency vibration is considered. The global spectral matrix can be expressed as

$$\mathbf{D}(\omega,\theta) = -\omega^2\mathbf{M}(\omega,\theta) + \mathrm{i}\omega\mathbf{C}(\omega,\theta) + \mathbf{K}(\omega,\theta) \in \mathbb{C}^{N\times N} \tag{21}$$

where N is the dynamic degrees of freedom. Following the proposed approach, in general the matrix $\mathbf{D}(\omega,\theta)$ can be expressed as

$$\mathbf{D}(\omega,\theta) = \mathbf{D}_0(\omega) + \sum_j \xi_j(\theta)\mathbf{D}_j(\omega) \tag{22}$$

In this equation $\mathbf{D} : (\Omega \times \Theta) \to \mathbb{C}^{N\times N}$ is a complex random symmetric matrix and it needs to be inverted for every ω to obtain the dynamic response. Here Ω denotes the space of frequency. Here direct Monte Carlo simulation is used to obtain the response statistics in the numerical examples to be followed.

3. Overview of deterministic dynamic stiffness method for undamped membranes

The stochastic dynamic stiffness method (SDSM) is developed based on the frequency-dependent exact shape function of a deterministic system. Therefore, this section is devoted to revisiting the exact dynamic stiffness formulation for an undamped membrane with general classical boundary conditions as developed very recently by the authors [42].

Consider a homogeneous and flexible membrane whose mass per unit area is ρ and is taut in x and y direction by T_x and T_y respectively, namely, as shown in Fig. 1. In the frequency domain, we have

$$\frac{\partial^2 U}{\partial x^2} + \beta\frac{\partial^2 U}{\partial y^2} + k^2 U = 0 \tag{23}$$

where $U = U(x,y)$ is the transverse displacement of the membrane and

$$\beta = \frac{T_y}{T_x}, k = \frac{\omega}{c_0}, c_0 = \sqrt{\frac{T_x}{\rho}} \tag{24}$$

In order to satisfy the three different principal boundary conditions (PBCs, as shown in Appendix A), the general solutions of Eq. (23) should take the forms as follows [42].

$$U(x,y) = \begin{cases} \sum_{m=1}^{\infty} U_m(x)\sin(\alpha_m y), & \mathrm{C}-\mathrm{C} \text{ or } \mathrm{C}-\mathrm{F} \\ \sum_{m=0}^{\infty} U_m(x)\cos(\alpha_m y), & \mathrm{F}-\mathrm{F} \end{cases} \tag{25}$$

with

$$\alpha_m = \begin{cases} \frac{m\pi}{l}, m = 1,2,3\cdots, & \mathrm{C}-\mathrm{C} \\ \frac{m\pi}{l}, m = 0,1,2\cdots, & \mathrm{F}-\mathrm{F} \\ \frac{(m-\frac{1}{2})\pi}{l}, m = 1,2,3\cdots, & \mathrm{C}-\mathrm{F} \end{cases} \tag{26}$$

where m denotes the half wave number of a rectangular membrane element in the y direction, $U_m(x)$ is derived in Appendix B. The external force applied normal to the surface of the membrane $P(x,y)$ can be expressed as

$$P(x,y) = T_x\frac{\partial U}{\partial x} = \begin{cases} \sum_{m=1}^{\infty} P_m(x)\sin(\alpha_m y) & \mathrm{C}-\mathrm{C} \text{ or } \mathrm{C}-\mathrm{F} \\ \sum_{m=0}^{\infty} P_m(x)\cos(\alpha_m y) & \mathrm{F}-\mathrm{F} \end{cases} \tag{27}$$

Based on exact shape functions, dynamic stiffness formulations for deterministic membrane elements can be derived as shown in Eq. (B.10), more details are referred to [42]. In order to derive the deterministic and random part of the element matrices, the shape function for a membrane element can be expressed in the form of Eq. (8) as shown in Eq. (B.12).

4. Stochastic dynamic stiffness formulation for damped membranes

Next, the exact shape functions of the deterministic undamped taut membrane are to be used to develop the stochastic dynamic stiffness formulations for damped membranes with uncertainties following the steps in Section 2.

4.1. Stochastic governing differential equation and random field discretization

If damping and stochastic nonhomogeneity are added to the membrane element shown in Fig. 1, then the governing differential equation (GDE) of a damped transversely vibrating membrane with stochastic material parameters can be described by

$$\begin{aligned} &\frac{\partial}{\partial x}\left(T_x(x,y)\frac{\partial u}{\partial x} + c_x\frac{\partial^2 u}{\partial x\partial t}\right) + \frac{\partial}{\partial y}\left(T_y(x,y)\frac{\partial u}{\partial y} + c_y\frac{\partial^2 u}{\partial y\partial t}\right) \\ &- c_\rho\frac{\partial u}{\partial t} - \rho(x,y)\frac{\partial^2 u}{\partial t^2} = 0 \end{aligned} \tag{28}$$

where $x \in [0,a]$ and $y \in [0,b]$ are given with respect to global axes placed in a corner of the rectangular element, c_x and c_y are Kelvin–Voigt (material) damping parameters [68] and c_ρ is viscous damping parameter, which are assumed to be deterministic constants. The GDE presented here is based on linear theory, which is limited to linear structural behavior and not directly applicable to nonlinear analysis under larger displacement. Moreover, the present theory is developed based on a rectangular membrane element, which is directly applicable to rectangular elements and their assemblies, but cannot be used to model more general geometries. In order to be applicable to more general geometries, other

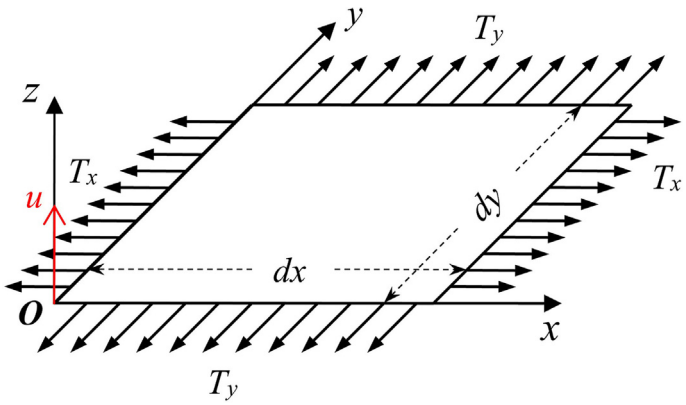

Fig. 1. Displacements and forces of a rectangular membrane element.

shapes of elements need to be developed. Now the three variables $T_x(x,y), T_y(x,y)$ and $\rho(x,y)$ are to be expanded with KL expansions. It should be noted that in the dynamic stiffness formulation, the origin is placed at a corner of the membrane element, while the KL expansion is to be performed at the centre of the membrane element. Therefore, global axes x and y are introduced for KL expansion with the following relation to x and y

$$\mathrm{x} = x - a/2, \qquad \mathrm{y} = y - b/2 \tag{29}$$

we can assume an exponentially decaying autocorrelation function for all three variables.

$$C(\mathrm{x}_1, \mathrm{x}_2; \mathrm{y}_1, \mathrm{y}_2) = e^{-|\mathrm{x}_1 - \mathrm{x}_2|/c_{xp} - |\mathrm{y}_1 - \mathrm{y}_2|/c_{yp}} \tag{30}$$

where $p = 1, 2, 3$ corresponds to the three parameters T_x, T_y and ρ, respectively. The exponential autocorrelation function in Eq. (30) has been widely used in the literature. However, this function is not differentiable at the origin. As a result, a large number of terms are necessary in the KL expansion. Spanos et. al. [69] proposed a modified exponential covariance kernel which circumvents this problem. In the current work, larger correlation lengths are considered and consequently the drawback of the autocorrelation function in Eq. (30) is avoided by considering higher-order terms in the KL expansions in both the directions.

Following the KL expansion in the coordinates x, y, considering n_{xp} number of terms in the x direction and n_{yp} number of terms in the y direction ($p = 1, 2, 3$ corresponds to the three parameters T_x, T_y and ρ, respectively), we have

$$T_x(\mathrm{x},\mathrm{y}) = T_{x0} + \sum_{i=1}^{n_{x1}/2n_{y1}/2} \sum_{j=1} \left(\xi_{ij1}\sqrt{\lambda_{ij1}}f_{ij1} + \xi_{i^*j1}\sqrt{\lambda_{i^*j1}}f_{i^*j1} + \xi_{ij^*1}\sqrt{\lambda_{ij^*1}}f_{ij^*1} + \xi_{i^*j^*1}\sqrt{\lambda_{i^*j^*1}}f_{i^*j^*1}\right) \tag{31}$$

$$T_y(\mathrm{x},\mathrm{y}) = T_{y0} + \sum_{i=1}^{n_{x2}/2n_{y2}/2} \sum_{j=1} \left(\xi_{ij2}\sqrt{\lambda_{ij2}}f_{ij2} + \xi_{i^*j2}\sqrt{\lambda_{i^*j2}}f_{i^*j2} + \xi_{ij^*2}\sqrt{\lambda_{ij^*2}}f_{ij^*2} + \xi_{i^*j^*2}\sqrt{\lambda_{i^*j^*2}}f_{i^*j^*2}\right) \tag{32}$$

$$\rho(\mathrm{x},\mathrm{y}) = \rho_0 + \sum_{i=1}^{n_{x3}/2n_{y3}/2} \sum_{j=1} \left(\xi_{ij3}\sqrt{\lambda_{ij3}}f_{ij3} + \xi_{i^*j3}\sqrt{\lambda_{i^*j3}}f_{i^*j3} + \xi_{ij^*3}\sqrt{\lambda_{ij^*3}}f_{ij^*3} + \xi_{i^*j^*3}\sqrt{\lambda_{i^*j^*3}}f_{i^*j^*3}\right) \tag{33}$$

with

$$\lambda_{ijp} = \frac{4c_{xp}c_{yp}}{\left(\omega_{ix}^2 + c_{xp}\right)\left(\omega_{jy}^2 + c_{yp}\right)}, \qquad f_{ijp} = \frac{\cos\left(w_i\mathrm{x}\right)}{\sqrt{a/2 + \frac{\sin\left(\omega_i a\right)}{2\omega_i}}} \frac{\cos\left(w_j\mathrm{y}\right)}{\sqrt{b/2 + \frac{\sin\left(\omega_j b\right)}{2\omega_j}}},$$

$$\lambda_{i^*jp} = \frac{4c_{xp}c_{yp}}{\left(\omega_{ix}^{*2} + c_{xp}\right)\left(\omega_{jy}^2 + c_{yp}\right)}, \qquad f_{i^*jp} = \frac{\sin\left(w_i^*\mathrm{x}\right)}{\sqrt{a/2 - \frac{\sin\left(\omega_i^* a\right)}{2\omega_i^*}}} \frac{\cos\left(w_j\mathrm{y}\right)}{\sqrt{b/2 + \frac{\sin\left(\omega_j b\right)}{2\omega_j}}},$$

$$\lambda_{ij^*p} = \frac{4c_{xp}c_{yp}}{\left(\omega_{ix}^2 + c_{xp}\right)\left(\omega_{jy}^{*2} + c_{yp}\right)}, \qquad f_{ij^*p} = \frac{\cos\left(w_i\mathrm{x}\right)}{\sqrt{a/2 + \frac{\sin\left(\omega_i a\right)}{2\omega_i}}} \frac{\sin\left(w_j^*\mathrm{y}\right)}{\sqrt{b/2 - \frac{\sin\left(\omega_j^* b\right)}{2\omega_j^*}}},$$

$$\lambda_{i^*j^*p} = \frac{4c_{xp}c_{yp}}{\left(\omega_{ix}^{*2} + c_{xp}\right)\left(\omega_{jy}^{*2} + c_{yp}\right)}, \qquad f_{i^*j^*p} = \frac{\sin\left(w_i^*\mathrm{x}\right)}{\sqrt{a/2 - \frac{\sin\left(\omega_i^* a\right)}{2\omega_i^*}}} \frac{\sin\left(w_j^*\mathrm{y}\right)}{\sqrt{b/2 - \frac{\sin\left(\omega_j^* b\right)}{2\omega_j^*}}} \tag{34}$$

where the constants T_{x0}, T_{y0} and ρ_0 in the baseline model satisfy Eq. (23) and $\lambda_{ijp}, f_{ijp} (i, j = 1, 2, 3, \cdots, p = 1, 2, 3)$ are the eigenvalues and eigenfunctions corresponding to the homogeneous Gaussian random fields with zero means and autocorrelation functions given by Eq. (30).

4.2. Stochastic dynamic stiffness matrices

Taking Eqs. (29)-(34) into consideration, the stochastic stiffness and mass matrix for a membrane element can be developed in the form

$$\mathbf{K}_e = \mathbf{K}_{e_0} + \sum_{i=1}^{n_{x1}/2n_{y1}/2} \sum_{j=1} \left(\xi_{ij1}\sqrt{\lambda_{ij1}}\mathbf{K}_{ex}^{ij} + \xi_{i^*j1}\sqrt{\lambda_{i^*j1}}\mathbf{K}_{ex}^{i^*j} + \xi_{ij^*1}\sqrt{\lambda_{ij^*1}}\mathbf{K}_{ex}^{ij^*} + \xi_{i^*j^*1}\sqrt{\lambda_{i^*j^*1}}\mathbf{K}_{ex}^{i^*j^*}\right) + \sum_{i=1}^{n_{x2}/2n_{y2}/2} \sum_{j=1} \left(\xi_{ij2}\sqrt{\lambda_{ij2}}\mathbf{K}_{ey}^{ij} + \xi_{i^*j2}\sqrt{\lambda_{i^*j2}}\mathbf{K}_{ey}^{i^*j} + \xi_{ij^*2}\sqrt{\lambda_{ij^*2}}\mathbf{K}_{ey}^{ij^*} + \xi_{i^*j^*2}\sqrt{\lambda_{i^*j^*2}}\mathbf{K}_{ey}^{i^*j^*}\right) \tag{35}$$

$$\mathbf{M}_e = \mathbf{M}_{e0} + \sum_{i=1}^{n_{x3}/2n_{y3}/2} \sum_{j=1} \left(\xi_{ij3}\sqrt{\lambda_{ij3}}\mathbf{M}_e^{ij} + \xi_{i^*j3}\sqrt{\lambda_{i^*j3}}\mathbf{M}_e^{i^*j} + \xi_{ij^*3}\sqrt{\lambda_{ij^*3}}\mathbf{M}_e^{ij^*} + \xi_{i^*j^*3}\sqrt{\lambda_{i^*j^*3}}\mathbf{M}_e^{i^*j^*}\right) \tag{36}$$

where $\mathbf{K}_{e_0}, \mathbf{M}_{e0}$ are the deterministic matrices obtained in the deterministic element and the rest are the random parts obtained by using the eigenfunctions. For the transverse vibration of the membrane under all three kinds of principal boundary conditions (PBCs, see Appendix A), they can be obtained as follows.

$$\mathbf{K}_{e0}(\omega) = \mathbf{\Gamma} \int_{x=0}^{a} \int_{y=0}^{b} \left\{ T_{x0} \left[\frac{\partial \mathbf{s}(x,y,\omega)}{\partial x}\right] \left[\frac{\partial \mathbf{s}(x,y,\omega)}{\partial x}\right]^T + T_{y0} \left[\frac{\partial \mathbf{s}(x,y,\omega)}{\partial y}\right] \left[\frac{\partial \mathbf{s}(x,y,\omega)}{\partial y}\right]^T \right\} \mathrm{d}y\mathrm{d}x\mathbf{\Gamma}^T \tag{37}$$

$$\mathbf{K}_{ex}^{ij}(\omega) = \mathbf{\Gamma} \int_{x=0}^{a} \int_{y=0}^{b} \left\{ f_{ij1} \left[\frac{\partial \mathbf{s}(x,y,\omega)}{\partial x}\right] \left[\frac{\partial \mathbf{s}(x,y,\omega)}{\partial x}\right]^T \right\} \mathrm{d}y\mathrm{d}x\mathbf{\Gamma}^T \tag{38}$$

$$\mathbf{K}_{ey}^{ij}(\omega) = \mathbf{\Gamma} \int_{x=0}^{a} \int_{y=0}^{b} \left\{ f_{ij2} \left[\frac{\partial \mathbf{s}(x,y,\omega)}{\partial y}\right] \left[\frac{\partial \mathbf{s}(x,y,\omega)}{\partial y}\right]^T \right\} \mathrm{d}y\mathrm{d}x\mathbf{\Gamma}^T \tag{39}$$

$$\mathbf{M}_{e0}(\omega) = \rho_0 \mathbf{\Gamma} \int_{x=0}^{a} \int_{y=0}^{b} \mathbf{s}(x,y,\omega)\mathbf{s}^T(x,y,\omega)\mathrm{d}y\mathrm{d}x\mathbf{\Gamma}^T \tag{40}$$

$$\mathbf{M}_e^{ij}(\omega) = \mathbf{\Gamma} \int_{x=0}^{a} \int_{y=0}^{b} f_{ij3}\mathbf{s}(x,y,\omega)\mathbf{s}^T(x,y,\omega)\mathrm{d}y\mathrm{d}x\mathbf{\Gamma}^T \tag{41}$$

where the derivation of $\mathbf{\Gamma}$ and $\mathbf{s}$ have been given in Eqs. (B.12)–(B.15) of Appendix B. Note that since damping coefficients are introduced for the stochastic system, Eq. (B.2) should be modified as follows.

$$\lambda = \sqrt{\beta_d \alpha_m^2 - k_d^2} \tag{42}$$

where

$$\beta_d = \frac{T_{y0} + \mathrm{i}c_y\omega}{T_{x0} + \mathrm{i}c_x\omega}, k_d = \frac{\omega}{c_d}, c_d = \sqrt{\frac{T_{x0} + \mathrm{i}c_x\omega}{\rho_0 - \mathrm{i}c_\rho/\omega}} \tag{43}$$

The rest can be derived in a similar way just by replacing ij with i^*j, ij^* and i^*j^*. Taking C-C PBCs for example, performing the above integrations through symbolic calculations, we will have

$$\mathbf{K}_{e0}(\omega)=\frac{1}{4\lambda\alpha_m}\left\{\lambda^2 T_{x0}(b\alpha_m-c_1 s)\begin{pmatrix} a\lambda\mathrm{Csh}^2+\mathrm{Cth} & -(a\lambda\mathrm{Cth}+1)\mathrm{Csh}\\ -(a\lambda\mathrm{Cth}+1)\mathrm{Csh} & a\lambda\mathrm{Csh}^2+\mathrm{Cth}\end{pmatrix}\right.$$
$$\left.+\alpha_m^2 T_{y0}(b\alpha_m+c_1 s)\begin{pmatrix} \mathrm{Cth}-a\lambda\mathrm{Csh}^2 & (a\lambda\mathrm{Cth}-1)\mathrm{Csh}\\ (a\lambda\mathrm{Cth}-1)\mathrm{Csh} & \mathrm{Cth}-a\lambda\mathrm{Csh}^2\end{pmatrix}\right\} \tag{44}$$

$$\mathbf{M}_{e0}(\omega)=\rho_0(b\alpha_m-c_1 s)\begin{pmatrix} \mathrm{Cth}-a\lambda\mathrm{Csh}^2 & (a\lambda\mathrm{Cth}-1)\mathrm{Csh}\\ (a\lambda\mathrm{Cth}-1)\mathrm{Csh} & \mathrm{Cth}-a\lambda\mathrm{Csh}^2\end{pmatrix} \tag{45}$$

$$\mathbf{K}_{ex}^{ij}(\omega)=\frac{2\lambda^2 k_{b1}^0\mathrm{Csh}^2}{\Delta_{00}}\begin{pmatrix} k_{a1}^0 & -2k_{a3}^0\\ -2k_{a3}^0 & k_{a1}^0\end{pmatrix},\quad \mathbf{K}_{ex}^{i^*j}(\omega)=\frac{2\lambda^2 k_{b1}^0\mathrm{Csh}}{\Delta_{10}}\begin{pmatrix} -k_{a1}^1 & 0\\ 0 & k_{a1}^1\end{pmatrix} \tag{46}$$

$$\mathbf{K}_{ex}^{ij^*}(\omega)=\frac{2\lambda^2 k_{b1}^1 s\mathrm{Csh}^2}{\Delta_{01}}\begin{pmatrix} k_{a1}^0 & -2k_{a3}^0\\ -2k_{a3}^0 & k_{a1}^0\end{pmatrix},\quad \mathbf{K}_{ex}^{i^*j^*}(\omega)=\frac{2\lambda^2 k_{b1}^1 s\mathrm{Csh}}{\Delta_{11}}\begin{pmatrix} -k_{a1}^1 & 0\\ 0 & k_{a1}^1\end{pmatrix} \tag{47}$$

$$\mathbf{K}_{ey}^{ij}(\omega)=-\frac{2k_{b2}^0\alpha_m^2\mathrm{Csh}^2}{\Delta_{00}}\begin{pmatrix} k_{a2}^0 & 2k_{a4}^0\lambda\\ 2k_{a4}^0\lambda & k_{a2}^0\end{pmatrix},\quad \mathbf{K}_{ey}^{i^*j}(\omega)=-\frac{2k_{b2}^0\alpha_m^2\mathrm{Csh}}{\Delta_{10}}\begin{pmatrix} -k_{a1}^1 & 0\\ 0 & k_{a1}^1\end{pmatrix} \tag{48}$$

$$\mathbf{K}_{ey}^{ij^*}(\omega)=-\frac{2k_{b1}^1 s\alpha_m^2\mathrm{Csh}^2}{\Delta_{01}}\begin{pmatrix} k_{a2}^0 & 2k_{a4}^0\lambda\\ 2k_{a4}^0\lambda & k_{a2}^0\end{pmatrix},\quad \mathbf{K}_{ey}^{i^*j^*}(\omega)=-\frac{2k_{b1}^1 s\alpha_m^2\mathrm{Csh}}{\Delta_{11}}\begin{pmatrix} -k_{a1}^1 & 0\\ 0 & k_{a1}^1\end{pmatrix} \tag{49}$$

$$\mathbf{M}_{ey}^{ij}(\omega)=\frac{2k_{b1}^0\mathrm{Csh}^2}{\Delta_{00}}\begin{pmatrix} k_{a2}^0 & 2k_{a4}^0\lambda\\ 2k_{a4}^0\lambda & k_{a2}^0\end{pmatrix},\quad \mathbf{M}_{ey}^{i^*j}(\omega)=\frac{2k_{b1}^0\mathrm{Csh}}{\Delta_{10}}\begin{pmatrix} -k_{a1}^1 & 0\\ 0 & k_{a1}^1\end{pmatrix} \tag{50}$$

$$\mathbf{M}_{ey}^{ij^*}(\omega)=\frac{2k_{b1}^1 s\mathrm{Csh}^2}{\Delta_{01}}\begin{pmatrix} k_{a2}^0 & 2k_{a4}^0\lambda\\ 2k_{a4}^0\lambda & k_{a2}^0\end{pmatrix},\quad \mathbf{M}_{ey}^{i^*j^*}(\omega)=\frac{2k_{b1}^1 s\mathrm{Csh}}{\Delta_{11}}\begin{pmatrix} -k_{a1}^1 & 0\\ 0 & k_{a1}^1\end{pmatrix} \tag{51}$$

where variables defined in Eqs. (44)–(51) are provied in detail in Appendix C.

For the case of C-F PBCs, the matrices take the same form as Eqs. (44)–(51) except for different α_m as defined in Eq. (26). While for F-F PBCs, α_m remain unchanged but $(b\alpha_m-c_1 s)$ and $(b\alpha_m+c_1 s)$ in Eq. (44) need swap places, $(b\alpha_m-c_1 s)$ in Eq. (45) should be $(b\alpha_m+c_1 s), k_{b1}^0$ in Eqs. (46) and (50) should be replaced by $-k_{b2}^0$, and k_{b2}^0 in Eq. (48) should be $-k_{b1}^0$, negative signs need to be added in front of the expressions of Eqs. (47), (49) and (51).

After obtaining the deterministic part and random part of the element stiffness and mass matrices, the dynamic stiffness matrix can be derived by Eq. (22). By using the stochastic dynamic stiffness matrix $\mathbf{D}(\omega,\theta)$, the dynamic response can be derived, which will be discussed in the next section.

5. Stochastic dynamic response analysis

Once the stochastic dynamic stiffness matrices $\mathbf{D}(\omega,\theta)$ for the membrane elements under one of the three kinds of principal boundary conditions (PBCs, see Appendix A) are obtained, they can be assembled for the overall membrane assembly. Upon applying prescribed BCs on the nodal boundaries (NBs, see Appendix A), we arrived at the global stochastic dynamic stiffness matrix $\mathbf{D}_m^f(\omega,\theta)$ for the final structure, where m denotes the half wave number in the y direction. The assembly procedure and the application of nodal boundary conditions are similar to those of plate assembly.

Therefore, forced vibration analysis of the membrane assemblies under any prescribed BCs can be performed based on

$$\mathbf{D}_m^f(\omega,\theta)\mathbf{d}_m^f=\mathbf{f}_m^f \tag{52}$$

where generalized forces $\mathbf{f}_m^f$ can be obtained by any prescribed transverse excitation $P(x,y)$ in the form of Eq. (27) by using the projection method.

For example, supposing two arbitrary excitations either concentrated or distributed applied at any arbitrary locations of the membrane assembly, as shown by $P_1(x,y)$ and $P_2(x,y)$ in Fig. 2, the equivalent nodal loads $\mathbf{f}^e$ caused by the excitations for each membrane element can be obtained through integration

$$\mathbf{f}^e=\int_x\int_y P(x,y)\mathbf{N}(x,y,\omega)dxdy \tag{53}$$

where $\mathbf{N}(x,y,\omega)$ is the shape function given in Eq. (B.12). Subsequently, the equivalent nodal loads can be superposed linearly on the elements' nodes. For each nodal load $P_i(y)$ under all three kinds of PBCs, according to Eq. (27) we have

$$P_i(y)=\begin{cases}\sum_{m=1}^{\infty}P_{mi}\sin(\alpha_m y) & \mathrm{C-C\ or\ C-F}\\ \sum_{m=0}^{\infty}P_{mi}\cos(\alpha_m y) & \mathrm{F-F}\end{cases} \tag{54}$$

Therefore, according to Eq. (54), the generalized force P_{mi} for a given wavenumber m can be expressed as

$$P_{mi}=\frac{2}{b}\int_0^b P_i(y)\sin(\alpha_m y)\mathrm{d}y, m=1,2,3,\cdots\quad \mathrm{C-C\ or\ C-F} \tag{55}$$

$$P_{mi}=\begin{cases}\frac{2}{b}\int_0^b P_i(y)\cos(\alpha_m y)\mathrm{d}y, m=1,2,3,\cdots, & \mathrm{F-F}\\ \frac{1}{b}\int_0^b P_i(y)\mathrm{d}y, m=0. & \mathrm{F-F}\end{cases} \tag{56}$$

After obtaining the generalized force P_{mi} on each of the NBs, the generalized force vector $\mathbf{f}_m^f$ can be developed in terms of nodal boundary conditions (NBCs, see Appendix A) prescribed beforehand. Then by solving Eq. (52), the generalized displacements $\mathbf{d}_m^f$ can be obtained. Substituting the generalized displacements d_{mi} on the NBs into Eq. (25) and taking inverse Fourier transformation, the dynamic response at any point along the NBs can be obtained as follows.

$$U_i^e(y_s)=\begin{cases}\sum_{m=1}^{\infty}d_{mi}\sin(\alpha_m y_s), & \mathrm{C-C\ or\ C-F}\\ \sum_{m=0}^{\infty}d_{mi}\cos(\alpha_m y_s), & \mathrm{F-F}\end{cases} \tag{57}$$

Further, once we obtain the generalized displacements d_{mi}, the nodal displacement vector $\mathbf{d}^e$ for each membrane element can be

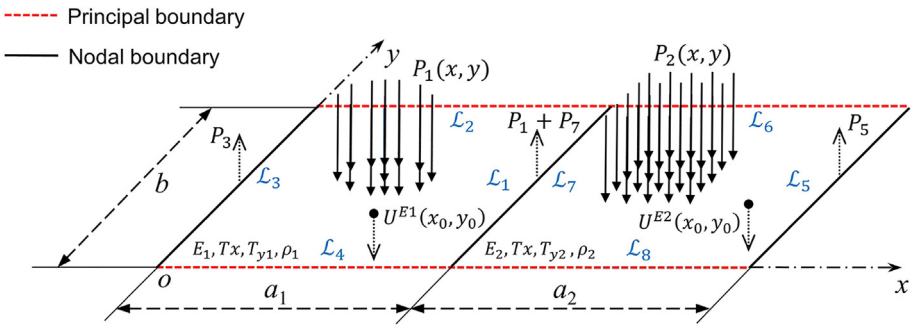

Fig. 2. The excitations either concentrated or distributed and responses at any arbitrary location of the membrane assembly.

easily developed. Eq. (25) now can be expressed in the form of the shape function (see Appendix B for details) as

$$U^e(x,y) = \begin{cases} \sum_{m=1}^{\infty} \mathbf{N}^T(x,y,\omega)\mathbf{d}^e, & \text{C}-\text{C or C}-\text{F} \\ \sum_{m=0}^{\infty} \mathbf{N}^T(x,y,\omega)\mathbf{d}^e, & \text{F}-\text{F} \end{cases} \tag{58}$$

According to Eq. (58), we can obtain the response of each membrane element at some arbitrary location (x_0, y_0) as shown in Fig. 2.

6. Results and discussions

To demonstrate the derivations proposed above, we consider a rectangular membrane as an illustrative example. The mean mass per unit area and tensions are assumed to be $\rho_0 = 7.805$ kg/m^2, $T_{x0} = 13800$ N/m, $T_{y0} = 6900$ N/m respectively. The length and width of the membrane are $a = 2m$ and $b = 1m$ respectively. An FCCC boundary condition is considered for the cases in the following two subsections (the boundary conditions are listed in the anticlockwise sense of $\mathscr{L}_1$-$\mathscr{L}_2$-$\mathscr{L}_3$-$\mathscr{L}_4$ as described in Appendix A). The standard deviations of the random fields for T_x, T_y and ρ are assumed to be 10% of the mean values of the random fields, so the 'strength parameters' are considered as $\epsilon_{T_x} = 0.1, \epsilon_{T_y} = 0.1$ and $\epsilon_\rho = 0.1$. Although Gaussian random variable is assumed here, this may not be a suitable choice for physical properties such as the mean mass per unit area and tensions which assume positive values only. There is a small probability that a physically unrealistic negative value may occur for these properties. The chances of such non-physical negative values are greatly reduced by employing a small randomness as used here. In Section 6.1, we consider the material parameters T_x, T_y and ρ as Gaussian random variables and discuss the statistics of the eigenvalues of undamped free vibration through the direct Monte Carlo simulation. In Section 6.2, the stochastic dynamic response of a damped membrane is obtained using the developed stochastic dynamic stiffness formulations.

6.1. Eigenvalue analysis with random variables

It is assumed that the tensions T_x, T_y and the mass per unit area ρ are uncertain variables so that $T_x = T_{x0}(1 + \epsilon_{T_x}\theta_1)$, $T_y = T_{y0}(1 + \epsilon_{T_y}\theta_2), \rho = \rho_0(1 + \epsilon_\rho\theta_3)$, and $\boldsymbol{\Theta} = \{\theta_1, \theta_2, \theta_3\}^T \in \mathbb{R}^3$ is a vector of uncorrelated standard Gaussian random variables with zero mean and unit standard deviation.

The computation procedure is described as follows. First, the samples of three independent Gaussian random variables $\theta_1, \theta_2, \theta_3$ are generated, then the dynamic stiffness matrix in Eq. (B.10) for each set of samples is obtained and the natural frequencies of an undamped membrane are computed directly by the Wittrick-Williams algorithm [42]. Through Monte Carlo simulation, a total of 1000 samples are computed to obtain the statistics and the probability density functions of the eigenvalues. The above procedures are implemented in MATLAB. To demonstrate the efficiency and accuracy of the present theory, a comparison is made with the finite element method (FEM) with the help of MATLAB generating random samples for the FEM.

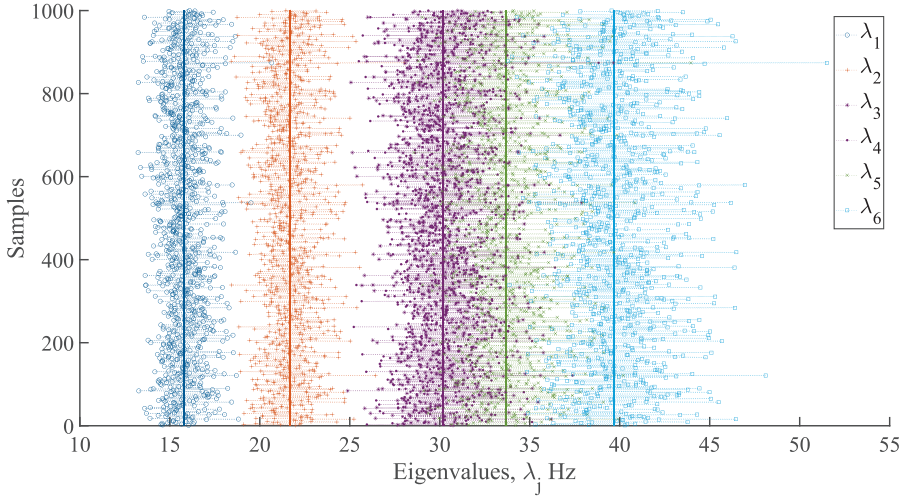

Fig. 3. Statistical scatter of the first six eigenvalues with parametric uncertainties (The third and the fourth eigenvalues have coincident deterministic natural frequency).

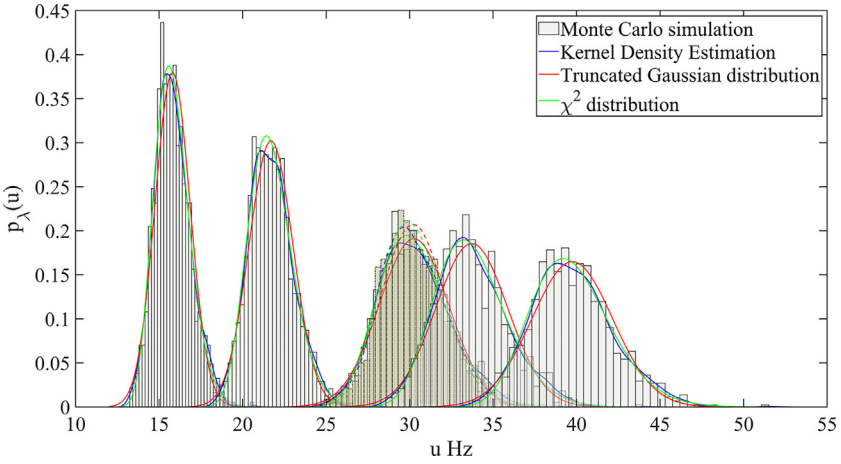

Fig. 4. Probability density functions of the first six eigenvalues (The third and the fourth eigenvalues have coincident deterministic natural frequency).

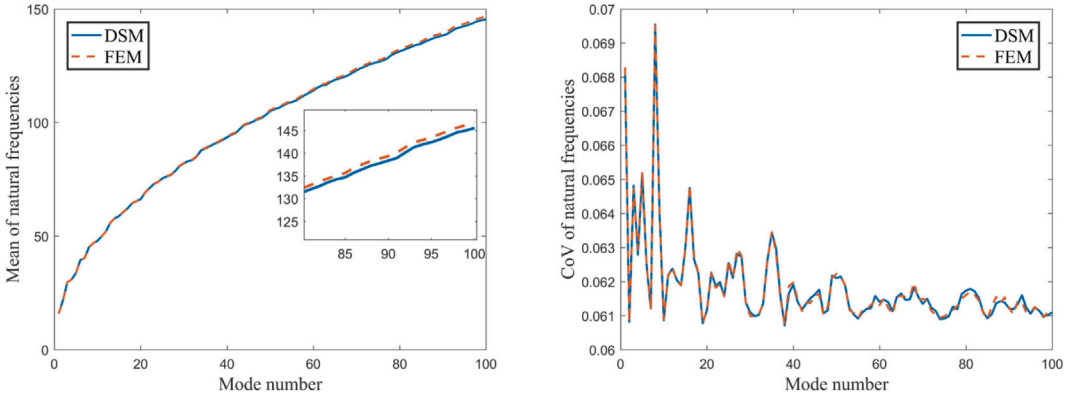

(a) mean (b) coefficient of variation (CoV)

Fig. 5. The mean and CoV of the first 100 natural frequencies based on MSC of 1000 samples.

Table 1
The means and coefficient of variations (CoV) of the eigenvalues with low to high frequency ranges based on MSC of 1000 samples (The results of FEM are obtained in ANSYS with 100×50 mesh size).

Mode	DSM		FEM	
	$\bar{f}$ (Hz)	CoV (%)	$\bar{f}$ (Hz)	CoV (%)
1	15.824	6.823	15.819	6.828
10	47.899	6.086	47.901	6.090
20	66.229	6.116	66.293	6.115
30	82.001	6.110	82.121	6.099
40	93.458	6.141	93.780	6.148
50	104.959	6.215	105.447	6.218
60	114.005	6.147	114.582	6.150
70	122.894	6.150	123.674	6.143
80	131.282	6.179	132.178	6.169
90	138.351	6.118	139.340	6.104
100	145.493	6.109	146.733	6.101
Time(min)	7		123	

The first six eigenvalues computed from Monte Carlo simulation by using 1000 samples are shown in Fig. 3. Solid lines represent the eigenvalues for the corresponding deterministic membrane model with average parameters, whose values are $\bar{\lambda}_1 = 15.768$ Hz, $\bar{\lambda}_2 = 21.671$ Hz, $\bar{\lambda}_3 = \bar{\lambda}_4 = 30.194$ Hz, $\bar{\lambda}_5 = 33.655$ Hz, $\bar{\lambda}_6 = 39.683$ Hz. While each random scatter denotes the eigenvalue of the corresponding random parameters with the given sample. It can be seen that the first two eigenvalues are well separated and little statistical overlap exists between them. However, the third to sixth eigenvalues are close to each other and there is distinct statistical overlap between them. Note that the third and the fourth eigenvalues have coincident deterministic natural frequency($\bar{\lambda}_3 = \bar{\lambda}_4$), their statistics are almost overlapping. Besides, the scatter degree becomes larger for higher modes than smaller modes, indicating that uncertainties in prestressing and mass distributions play a more important role for higher modes.

The probability density functions (pdf) of the first six eigenvalues obtained by the kernel density estimation, truncated Gaussian distribution and χ^2 distribution are shown in Fig. 4. The three different pdfs have been proposed in Appendix D. Meanwhile, normalized histograms of the eigenvalues obtained from the Monte Carlo simulation are provided in the same figure. It can be seen that those methods agree well with the Monte Carlo simulation results; There is a relatively small region of statistical overlap between the first and the second eigenvalues, while the regions of statistical overlap are significant among the last four of the six eigenvalues. It is worth mentioning that the region is almost coincident between the third and fourth eigenvalues because they correspond to coincident natural frequencies. The above discussions agree well with the observations based on Fig. 3.

To observe the statistics of the eigenvalues in a wide frequency range, we calculate the mean and the coefficient of variation (CoV) of the first 100 natural frequencies of the corresponding random

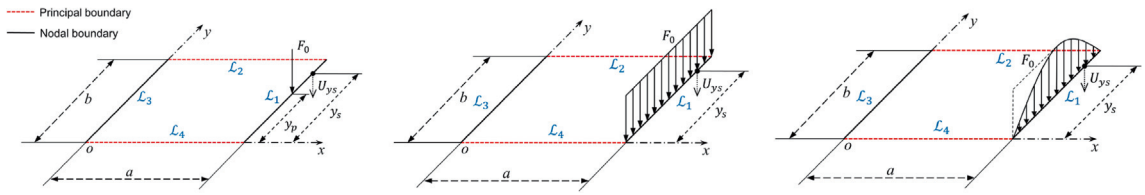

(a) concentrated excitation (b) uniform excitation (c) half-sine excitation

Fig. 6. Three different types of harmonic excitations applied at the nodal boundary of a rectangular membrane.

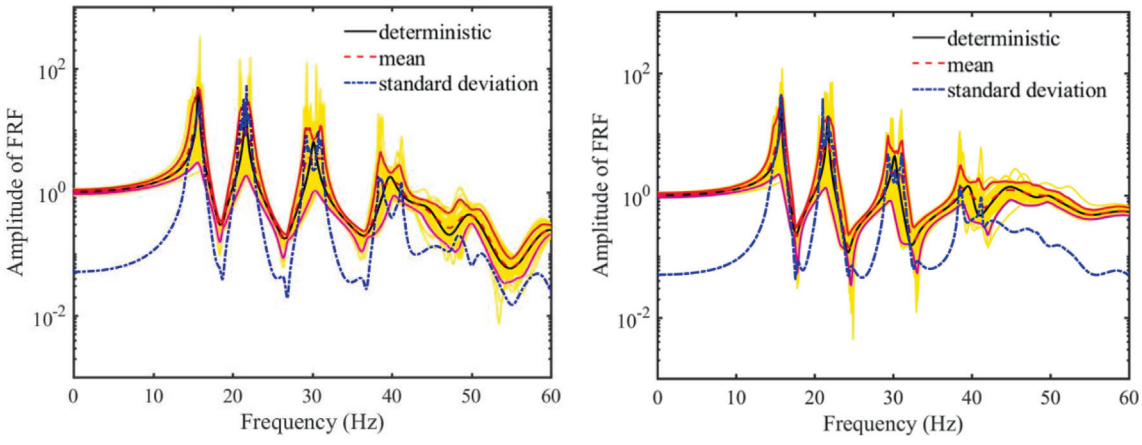

(a) uniformly distributed excitation (b) concentrated excitation

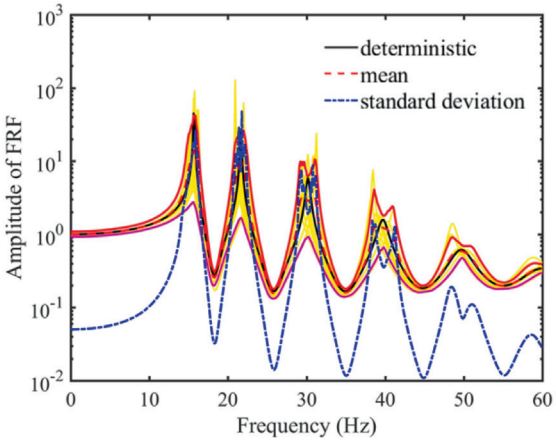

(c) half-sine excitation

Fig. 7. The amplitudes of dynamic responses at the midpoint of the free edge ($x = a, y = b/2$) under three different types of harmonic excitation. (The yellow curves represent the responses of the first 50 samples. The red and pink solid line exhibits the 5 and 95 percentile respectively.) (For interpretation of the references to colour in this figure legend, the reader is referred to the web version of this article.)

parameters with the given samples by using the DSM and FEM (the mesh size is 100×50), as shown in Fig. 5. The CoV is measured as the ratio of the standard deviation to the mean of the natural frequency. In general, the CoVs of the first 100 natural frequencies range from 6% up to 7%, and the differences of the CoVs are relatively small in higher frequency range. It might be due to the reason that the system parameters are assumed to be Gaussian random variables, the mean values are close to the nominal values. As can be seen from Fig. 5, the results computed by the DSM and FEM agree well for lower frequency range. However, the difference becomes larger for higher modes. This can be clearly illuminated from Table 1. However, the FEM takes as long as 123 min to compute the first 100 modes for a total of 1000 samples while the DSM only costs 7 min. It is apparent that the developed method gives results covering low to high frequency ranges with much higher accuracy and computational efficiency than the FEM.

6.2. Dynamic response analysis with random fields

In this subsection, the dynamic response analysis of a damped membrane is considered. The damping coefficients are set to be

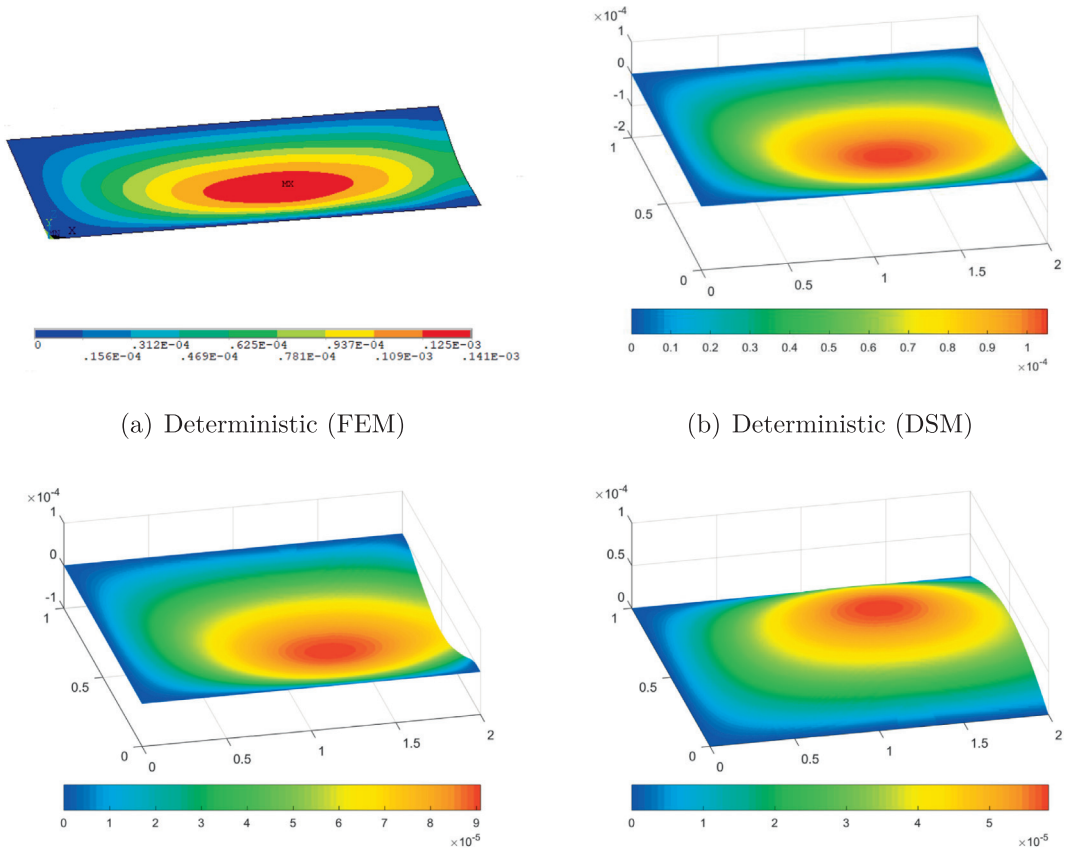

(a) Deterministic (FEM) (b) Deterministic (DSM)

(c) Mean (d) Standard deviation (Std)

Fig. 8. Displacement response field at 17.25 Hz under a uniformly distributed excitation.

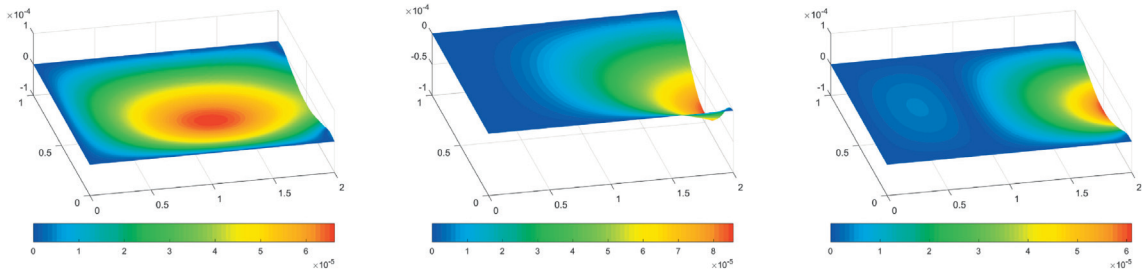

(a) Stochastic sample 1 (b) Stochastic sample 2 (c) Stochastic sample 3

Fig. 9. Stochastic samples of the displacement response fields at 17.25 Hz under a uniformly distributed excitation.

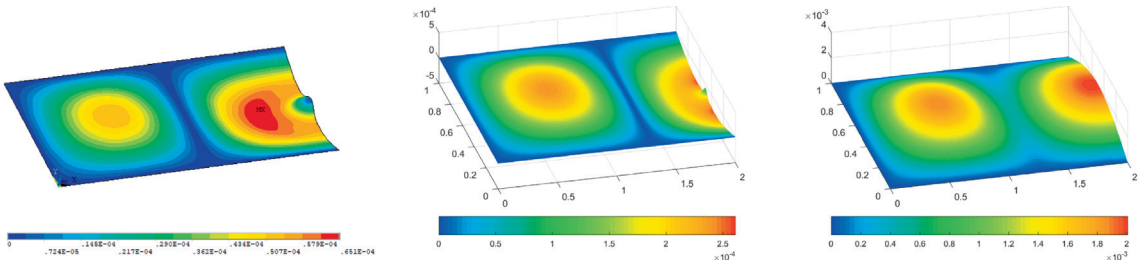

(a) Deterministic (FEM) (b) Mean (c) Standard deviation (Std)

Fig. 10. Displacement response field at 22.1 Hz under concentrated excitation.

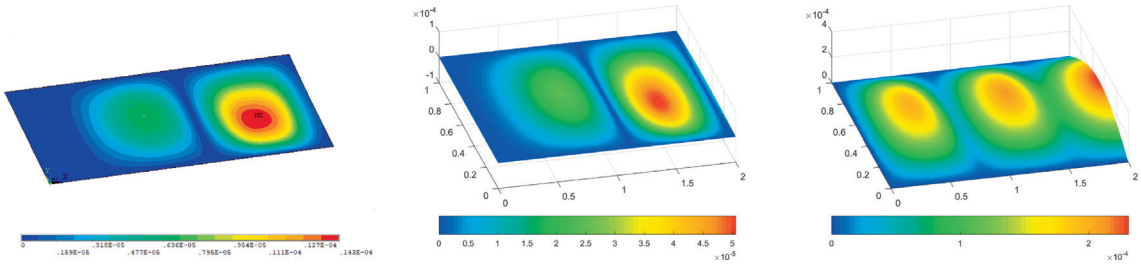

(a) Deterministic (FEM) (b) Mean (c) Standard deviation (Std)

Fig. 11. Displacement response field at 30.2 Hz under half-sine excitation.

$c_x = 5 \times 10^{-4}$ (s)$T_{x0}, c_y = 5 \times 10^{-4}$ (s)T_{y0} and $c_\rho = 3$ (s^{-1}) ρ_0. The correlation lengths of the random fields for T_x, T_y and ρ are assumed to be $a/2$ in x direction and $b/2$ in y direction. In general, we consider three types of boundary excitations including concentrated, uniform and half-sin with amplitudes of 1 N, 1 N/m and $\sin(\frac{\pi y}{b})$N/m respectively, as shown in Fig. 6. Those cases are probably the most representative cases in engineering applications.

Particularly, Dirac delta function will be introduced to describe concentrated excitation as shown in Fig. 6(a). As a consequence, $P(y)$ can be expressed as $P(y) = F_0\delta(y - y_p)$. Substituting it into Eq. (55), P_m can be derived as $P_m = 2F_0/b \sin(\alpha_m y_p)$.

Following the derivations in Sections 4 and 5, the response can be readily computed under the aforementioned three types of harmonic excitations. The response is computed up to 60 Hz covering the first sixteen natural modes of the membrane. In the calculation of response by DSM, the truncation number M for the series in Eq. (25) is taken to be 10 after convergence check.

The deterministic response, the mean, and the standard deviation of the absolute value of the response at the midpoint of the free edge $(x = a, y = b/2)$ under three types of excitations are shown in Fig. 7. To obtain these results, we use a Monte Carlo simulation by generating 2000 samples. In the KL expansion, 18 terms are used for both x and y directions. With 18 number of terms, the ratio of the last eigenvalue in the KL expansion to the first eigenvalue decreases to below 5% in both the directions. The element matrices incorporated with 18 random variables are obtained by the formulations derived in Section 4. In both cases under the uniform and half-sine excitations, the truncating number is set to be 10 and 1 respectively; while in the case under concentrated excitation, the truncating number is set to be 25 to assure sufficient convergence of the response below 60 Hz.

Some meaningful observations can be made based on Fig. 7. In all three cases, there are some discrepancies between the means of responses and the deterministic responses at lower frequencies, however, they are almost coincident at high frequencies. As for the standard deviations of the responses in the three cases, they are biased by the means and some peaks are reached around the natural frequencies. As the frequency increases, the standard deviation curves become flat. These results are obtained by using an individual dynamic stiffness element, and the calculation for the assembly of membrane elements with different material properties of the baseline models is also practical.

The results are shown in Fig. 7 focus on the response of a single point $(x = a, y = b/2)$ at the free edge. However, sometimes we are more concerned with the displacement response field of the whole structural domain. To shed light on the response over the whole domain, Figs. 8, 10 and 11 show the deterministic, mean and standard deviation (std) of the displacement response field under the aforementioned three types of excitations and three different frequencies.

The statistics of displacement response field at 17.25 Hz under the uniformly distributed excitation 1 N/m along the righthand-side boundary are shown in Fig. 8. The number of superposed waves in the DSM is 10 whereas the mesh in the FEM is 400 $\times$ 200. The deterministic response of displacement fields computed by the DSM and the FEM are in good agreement, which is evident by comparing Figs. 8(a) and 8(b). It can be seen that the mean and std of the displacement field (Fig. 8(c), (d)) shows the similar shape with that of the deterministic response of displacement field (Fig. 8 (b)) but with different amplitudes, and the std (Fig. 8(d)) is large where the amplitude is large. Besides, Fig. 9 provides the responses of membrane subject to uniform boundary excitations for three different random samples. It can be seen that the displacement response fields of the majority of samples follow similar patterns to the deterministic one (due to the fact that the shapes in Fig. 9a) and Fig. 8(c) are similar), whereas a few samples have different shapes as shown in Fig. 9(b), (c).

The displacement response fields at 22.1 Hz under concentrated excitation and 30.2 Hz under half-sine excitation along the righthand-side boundary are shown in Figs. 10 and 11. Figs. 10(a) and 11(a) represent the deterministic value computed by the FEM, while the rest are the means and standard deviations computed by the proposed method. The numbers of superposed waves in the DSM are 25 for concentrated excitation and 1 for half-sine excitation respectively. The mesh sizes of FEM in both cases are both 400 $\times$ 200. As can be seen in the figures, the distributions of the means and stds follow similar patterns to the deterministic displacement fields. But the mean values over the whole structural domain are different from the amplitudes of the deterministic displacement fields.

7. Conclusions

An analytical stochastic dynamic stiffness method (SDSM) is developed for the dynamic behavior of the bidirectionally taut damped membranes with distributed parametric uncertainties. The complex (due to damping) frequency-dependent two-dimensional transcendental shape functions coming from the DSM model are employed. The shape functions associated with the two-dimensional Karhunen–Loéve expansion representing the random fields are used to derive the explicit and exact closed-form expressions for the complex mass and stiffness matrix elements. By using the developed stochastic dynamic stiffness matrix in terms of the mass and stiffness matrix and a superposition technique, the exact closed-form expressions for the stochas-

tic dynamic responses of a single point and the global structural domain of a damped membranes are derived. Three typical types of excitations are considered to obtain the stochastic dynamic responses numerically. Some novel aspects presented in this paper for the first-time are:

- The analytical stochastic dynamic stiffness matrix of a two-dimensional structure (membrane) is developed for the first time by incoporating the Karhunen–Loéve expansion and the dynamic stiffness method.
- The DoF of the stochastic model is significantly reduced by using spectral discretization in random field, spectral model in frequency domain as well as spectral discretization of spatial deformation, which make it possible to solve the two-dimensional stochastic problems.
- The frequency-dependent shape functions are used which make the model to be valid for the whole frequency range, which is in sharp contrast to the stochastic finite element method suitable only for low frequency range.

Numerical examples are given to illustrate the computational efficiency and accuracy of the developed formulations, which leads to a unique competence to perform the efficient and reliable stochastic analysis for the whole frequency range compared with the conventional FEM. The approach proposed here can serve as the benchmark for extending stochastic dynamic stiffness method to more general two-dimensional structures such as plates [70,71] and composite panels [72–74].

Declaration of Competing Interest

The authors declare that they have no known competing financial interests or personal relationships that could have appeared to influence the work reported in this paper.

Acknowledgements

XL acknowledges the financial supports from the National Natural Science Foundation of China (Grant No. 11802345) and State Key Laboratory of High Performance Complex Manufacturing (Grant No. ZZYJKT2019-07). SA and XL also acknowledges the financial support from the High-end foreign expert introduction project through Grant no G20190018004.

Appendix A. Boundary conditions for the membrane

Fig. A1 shows displacement and force boundary conditions (BCs) on four edges of a rectangular membrane, where a and b are the length and width, respectively. P_2, U_2 and P_4, U_4 are the principal boundary conditions (PBCs) along the principal boundaries (PBs) $\mathscr{L}_2$ and $\mathscr{L}_4$ while P_1, U_1 and P_3, U_3 are the nodal boundary conditions (NBCs) along the nodal boundaries (NBs) $\mathscr{L}_1$ and $\mathscr{L}_3$. Note that the principal boundary means the opposite edge's boundary conditions are assumed to be known to derive exact general solutions of the membrane vibration, while the nodal boundary can be used to assemble the membrane assemblies and we can apply any arbitrary classical BCs onto it.

For a membrane element, there are three combinations for the PBCs: C-C, C-F(F-C), F-F as shown in Fig. A2, where C-F and F-C are equivalent (Note that a single membrane element also has three combinations for the NBCs: C-C, C-F(F-C), F-F. Hence, there are in total nine combinations of BCs for a rectangular membrane: CCCC, FCFC, FCCC, FFFF, CFCF, FFCF, CCCF, FCFF, FCCF, where the boundary conditions are listed in the anticlockwise sense of $\mathscr{L}_1$-$\mathscr{L}_2$-$\mathscr{L}_3$-$\mathscr{L}_4$). The fixed or clamped edge is denoted by the letter 'C' and the free edge is represented by the letter 'F'. For a clamped edge, $U_i = 0 (i = 1, 2, 3, 4)$. For a free edge, $P_i = 0 (i = 1, 2, 3, 4)$.

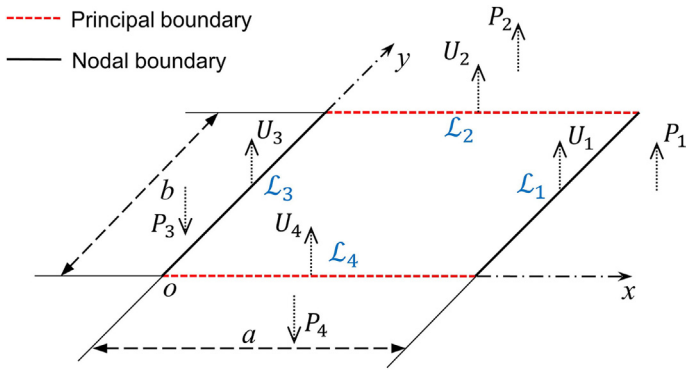

Fig. A1. Boundary conditions applied on four edges of a rectangular membrane.

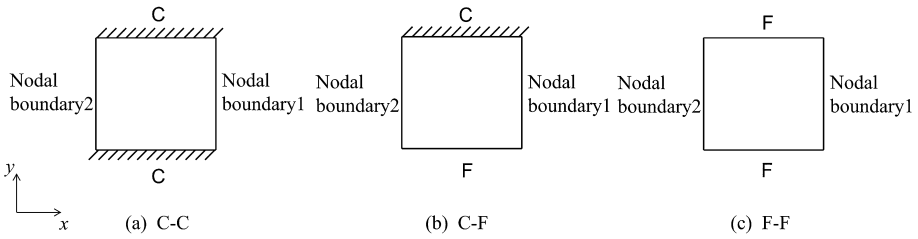

Fig. A2. Three combinations of principal boundary conditions (PBCs) for a rectangular membrane element.

Appendix B. Dynamic stiffness formulation for a deterministic undamped membrane

The derivation leading to Eq. (B.10) has been given in [42], we record here for the sake of self-completeness. Substituting Eq. (25) into Eq. (23) gives

$$\frac{\mathrm{d}^2 U_m}{\mathrm{d}x^2} - \lambda^2 U_m = 0 \tag{B.1}$$

where

$$\lambda = \sqrt{\beta\alpha_m^2 - k^2} \tag{B.2}$$

The general solution of Eq. (B.1) and $P_m(x)$ in Eq. (27) can be written as

$$U_m = C_1 \sinh(\lambda x) + C_2 \cosh(\lambda x) \tag{B.3}$$

$$P_m(x) = T_x\lambda(C_1 \cosh(\lambda x) + C_2 \sinh(\lambda x)) \tag{B.4}$$

where C_1 and C_2 are constants.

The displacement and force BCs on the nodal boundaries (NBs) can be recast as follows.

$$\text{At} \quad x = 0 : U_m = U_{m3} \qquad \text{At} \quad x = a : U_m = U_{m1} \tag{B.5}$$

$$\text{At} \quad x = 0 : P_m = -P_{m3} \qquad \text{At} \quad x = a : P_m = P_{m1} \tag{B.6}$$

Substituting Eqs. (B.5) and (B.6) into Eqs. (B.3) and (B.4), we have

$$\boldsymbol{d}^e = \begin{Bmatrix} U_{m1} \\ U_{m3} \end{Bmatrix} = \begin{bmatrix} \sinh\lambda a & \cosh\lambda a \\ 0 & 1 \end{bmatrix} \begin{Bmatrix} C_1 \\ C_2 \end{Bmatrix} \tag{B.7}$$

$$\boldsymbol{f}^e = \begin{Bmatrix} P_{m1} \\ P_{m3} \end{Bmatrix} = T_x\lambda \begin{bmatrix} \cosh\lambda a & \sinh\lambda a \\ -1 & 0 \end{bmatrix} \begin{Bmatrix} C_1 \\ C_2 \end{Bmatrix} \tag{B.8}$$

Eliminating the constant vector from Eqs. (B.7) and (B.8), the relationship between force vector $\boldsymbol{f}^e$ and displacement vector $\boldsymbol{d}^e$ can be established in the form of dynamic stiffness matrix $\boldsymbol{K}^e(\omega)$ as

$$\boldsymbol{f}^e = \boldsymbol{K}^e(\omega)\boldsymbol{d}^e \tag{B.9}$$

where

$$\boldsymbol{K}^e(\omega) = T_x\lambda \begin{bmatrix} \coth(\lambda a) & -\mathrm{csch}(\lambda a) \\ -\mathrm{csch}(\lambda a) & \coth(\lambda a) \end{bmatrix} \tag{B.10}$$

The derivation of Eqs. (B.1)–(B.10) above is applicable to the membrane elements under all three kinds of PBCs in Eq. (25).

According to Eq. (25), the two-dimensional displacement field can be represented by the linear combination of the basic functions. Eliminating the constant vector from Eqs. (B.7) and (25) to give the relationship between the displacement field and nodal displacement in the form of Eqs. (7) and (8).

$$U(x,y) = \mathbf{N}^T(x,y,\omega)\mathbf{d}^e \tag{B.11}$$

where $\mathbf{N}(x,y,\omega)$ is the frequency-dependent shape functions vector and can be expressed as

$$\mathbf{N}(x,y,\omega) = \boldsymbol{\Gamma}(\omega)\mathbf{s}(x,y,\omega) \tag{B.12}$$

In the above equation

$$\mathbf{s} = \begin{pmatrix} \sinh(\lambda x)\sin(\alpha_m y) \\ \cosh(\lambda x)\sin(\alpha_m y) \end{pmatrix}, \quad \mathrm{C}-\mathrm{C} \text{ or } \mathrm{C}-\mathrm{F} \tag{B.13}$$

$$\mathbf{s} = \begin{pmatrix} \sinh(\lambda x)cos(\alpha_m y) \\ \cosh(\lambda x)\cos(\alpha_m y) \end{pmatrix}, \qquad \mathrm{F}-\mathrm{F} \tag{B.14}$$

$$\boldsymbol{\Gamma}(\omega) = \begin{pmatrix} -\coth(\lambda a) & 1 \\ \mathrm{csch}(\lambda a) & 0 \end{pmatrix}, \quad \mathrm{C}-\mathrm{C}, \mathrm{C}-\mathrm{F}, \mathrm{F}-\mathrm{F} \tag{B.15}$$

Appendix C. Variables in Eqs. (44)–(51)

$$k_{a1}^0 = 2c_a^0\lambda\omega_i \mathrm{ChSh} + \left(\mathrm{Ch}^2 + 1\right)s_a^0\omega_i^2 + 4\lambda^2 s_a^0, \tag{C.1}$$

$$k_{b1}^0 = 2c_1c_b^0 s\omega_j\alpha_m + s^2 s_b^0\omega_j^2 - 4s_b^0\alpha_m^2, \tag{C.2}$$

$$k_{b2}^0 = -(c_1^2 + 1)s_b^0\omega_j^2 + 2c_1c_b^0 s\omega_j\alpha_m + 4s_b^0\alpha_m^2, \tag{C.3}$$

$$k_{a2}^0 = 2c_a^0\lambda\omega_i \mathrm{ChSh} + s_a^0\omega_i^2\mathrm{Sh}^2 - 4\lambda^2 s_a^0, \tag{C.4}$$

$$k_{a3}^0 = c_a^0\lambda\omega_i \mathrm{Sh} + s_a^0\omega_i^2\mathrm{Ch} + 2\lambda^2 s_a^0\mathrm{Ch}, \tag{C.5}$$

$$k_{a4}^0 = 2\lambda s_a^0\mathrm{Ch} - c_a^0\omega_i\mathrm{Sh}, \tag{C.6}$$

$$k_{a1}^1 = 2\lambda s_a^1\mathrm{Ch} - c_a^1\omega_i^*\mathrm{Sh}, \tag{C.7}$$

$$k_{b1}^1 = c_b^1 s\omega_j^* - 2c_1 s_b^1\alpha_m, \tag{C.8}$$

$$s = \sin(b\alpha_m), c_1 = \cos(b\alpha_m), \tag{C.9}$$

$$\mathrm{Ch} = \cosh(a\lambda), \mathrm{Sh} = \sinh(a\lambda), \mathrm{Cth} = \coth(a\lambda), \mathrm{Csh} = \mathrm{csch}(a\lambda), \tag{C.10}$$

$$s_a^0 = \sin\left(\frac{a\omega_i}{2}\right),$$

$$s_a^1 = \sin\left(\frac{1}{2}a\omega_i^*\right),$$

$$\Delta_{00} = Q_a^0 Q_b^0\left(4\lambda^2\omega_i + \omega_i^3\right)\left(\omega_j^3 - 4\omega_j\alpha_m^2\right), \tag{C.13}$$

$$\Delta_{01} = Q_a^1 Q_b^0\left(\omega_i^{*2} + 4\lambda^2\right)\left(\omega_j^3 - 4\omega_j\alpha_m^2\right), \tag{C.14}$$

$$\Delta_{10} = Q_a^0 Q_b^1\omega_i\left(\omega_i^2 + 4\lambda^2\right)\left(4\alpha_m^2 - \omega_j^{*2}\right), \tag{C.15}$$

$$\Delta_{11} = Q_a^1 Q_b^1\left(\omega_i^{*2} + 4\lambda^2\right)\left(4\alpha_m^2 - \omega_j^{*2}\right), \tag{C.16}$$

$$Q_a^0 = \sqrt{\frac{\sin(a\omega_i)}{\omega_i} + a},$$

$$Q_a^1 = \sqrt{a - \frac{\sin(a\omega_i^*)}{\omega_i^*}},$$

Appendix D. Probability density function of the eigenvalues

Three different kinds of methods named the kernel density estimation, truncated Gaussian distribution and χ^2 distribution are introduced in brief. They are applied in Section 4.1 to obtain the probability density functions (pdf) of eigenvalues.

1. Kernel distribution
   A kernel distribution is a nonparametric estimation method used for the pdf of a random variable. By selecting a smoothing function and a proper bandwidth value, a kernel distribution can be obtained. The kernel density estimator which represents the estimated pdf of a random variable can be expressed as

   $$p_{\lambda_j h}(u) = \frac{1}{nh}\sum_{i=1}^{n} K\left(\frac{u - u_i}{h}\right) \tag{D.1}$$

   where $u_1, u_2, \ldots, u_n$ are random samples of the eigenvalues, n is the sample size, $K(\cdot)$ is the kernel function, and h is the bandwidth. The associated default parameters are set in the MATLAB.
2. Truncated Gaussian distribution
   The truncated Gaussian density function takes the following form [75]

$$p_{\lambda_j}(u) = \frac{1}{\sqrt{2\pi}\sigma_j \Phi\left(\widehat{\lambda}_j/\sigma_j\right)} \exp\left\{-\frac{\left(u-\widehat{\lambda}_j\right)^2}{2\sigma_j^2}\right\}, \quad u \geqslant 0 \tag{D.2}$$

where $\widehat{\lambda}_j$ is the mean of the eigenvalues and σ_j is the standard deviation given by

$$\sigma_j^2 = \mu_j^{(2)} - \widehat{\lambda}_j^2 \tag{D.3}$$

In Section 4.1, the samples are generated through the Monte Carlo simulation, therefore, $\widehat{\lambda}_j$ and σ_j in Eq. (D.2) are represented by the sample means and standard deviations.

3. χ^2 distribution

The χ^2 probability density function can be expressed as following form [75]

$$p_{\lambda_j}(u) \approx \frac{1}{\gamma_j} p_{\chi^2_{\upsilon_j}}\left(\frac{u-\eta_j}{\gamma_j}\right) = \frac{\left(u-\eta_j\right)^{\upsilon_j/2-1} \exp\left\{-\left(u-\eta_j\right)/2\gamma_j\right\}}{\left(2\gamma_j\right)^{\upsilon_j/2}\Gamma\left(\upsilon_j/2\right)} \tag{D.4}$$

with

$$\eta_j = \frac{\mu_j^{(1)^2}\mu_j^{(2)} - 2\mu_j^{(2)^2} + \mu_j^{(1)}\mu_j^{(3)}}{2\mu_j^{(1)^3} - 3\mu_j^{(1)}\mu_j^{(2)} + \mu_j^{(3)}}$$
$$\gamma_j = \frac{2\mu_j^{(1)^3} - 3\mu_j^{(1)}\mu_j^{(2)} + \mu_j^{(3)}}{4\left(\mu_j^{(2)} - \mu_j^{(1)^2}\right)} \tag{D.5}$$

and

$$\upsilon_j = 8\frac{\left(\mu_j^{(2)} - \mu_j^{(1)^2}\right)^3}{\left(2\mu_j^{(1)^3} - 3\mu_j^{(1)}\mu_j^{(2)} + \mu_j^{(3)}\right)^2} \tag{D.6}$$

In Section 4.1, the constants η_j, γ_j, and υ_j are obtained by the first three moments of λ_j and the moments of the $\lambda_j(x)$ are estimated by the sample moments.

References

[1] Li D, Zheng ZL, Yang R, Zhang P. Analytical solutions for stochastic vibration of orthotropic membrane under random impact load. Materials 11 (7).
[2] Faes MG, Valdebenito MA, Moens D, Beer M. Bounding the first excursion probability of linear structures subjected to imprecise stochastic loading. Comput Struct 2020;239:106320.
[3] Kumar A, Saha SK, Matsagar VA. Stochastic response analysis of elastic and inelastic systems with uncertain parameters under random impulse loading. J Sound Vib 2019;461:114899.
[4] Hien TD, Noh HC. Stochastic isogeometric analysis of free vibration of functionally graded plates considering material randomness. Comput Methods Appl Mech Eng 2017;318:845–63.
[5] Stefanou G, Papadrakakis M. Stochastic finite element analysis of shells with combined random material and geometric properties. Comput Methods Appl Mech Eng 2004;193(1–2):139–60.
[6] Guedri M, Lima AM, Bouhaddi N, Rade DA. Robust design of viscoelastic structures based on stochastic finite element models. Mech Syst Signal Process 2010;24(1):59–77.
[7] Van den Nieuwenhof B, Coyette JP. Modal approaches for the stochastic finite element analysis of structures with material and geometric uncertainties. Comput Methods Appl Mech Eng 2003;192(33–34):3705–29.
[8] Xia B, Yu D, Liu J. Transformed perturbation stochastic finite element method for static response analysis of stochastic structures. Finite Elem Anal Des 2014;79:9–21.
[9] Sepahvand K. Spectral stochastic finite element vibration analysis of fiber-reinforced composites with random fiber orientation. Compos Struct 2016;145:119–28.
[10] Chen NZ, Guedes Soares C. Spectral stochastic finite element analysis for laminated composite plates. Comput Methods Appl Mech Eng 2008;197(51–52):4830–9.
[11] Kamiński M. Potential problems with random parameters by the generalized perturbation-based stochastic finite element method. Comput Struct 2010;88 (7–8):437–45.
[12] Pryse SE, Adhikari S. Stochastic finite element response analysis using random eigenfunction expansion. Comput Struct 2017;192:1–15.
[13] Jiang L, Liu X, Xiang P, Zhou W. Train-bridge system dynamics analysis with uncertain parameters based on new point estimate method. Eng Struct 2019;199:109454. https://doi.org/10.1016/j.engstruct.2019.109454.
[14] Liu X, Jiang LZ, Xiang P. Stochastic finite element method based on point estimate and Karhunen-Loéve expansion, Arch Appl Mech. doi:10.1007/s00419-020-01819-8.
[15] Vadlamani S, Arun CO. A stochastic B-spline wavelet on the interval finite element method for beams. Comput Struct 2020;233:106246.
[16] Zakian P, Khaji N, Kaveh A. Graph theoretical methods for efficient stochastic finite element analysis of structures. Comput Struct 2017;178:29–46.
[17] Han Z, Yu T, Phan H, Bui TQ. Extended stochastic finite element method enhanced by local mesh refinement for random voids analysis. Comput Struct 2020;239:106326.
[18] Feng N, Zhang G, Khandelwal K. On the performance evaluation of stochastic finite elements in linear and nonlinear problems. Comput Struct 2021;243:106408.
[19] Pranesh S, Ghosh D. A FETI-DP based parallel hybrid stochastic finite element method for large stochastic systems. Comput Struct 2018;195:64–73.
[20] Kaminski M. Stochastic perturbation approach to engineering structure vibrations by the finite difference method. J Sound Vib 2002;251(4):651–70.
[21] Vilmann O, Dasgupta G. Fundamental solutions of Mindlin plates with variable thickness for stochastic boundary elements. Eng Anal Bound Elem 1992;9 (1):47–59.
[22] Kaljevic I, Saigal S. Stochastic boundary elements for two-dimensional potential flow in homogeneous domains. Int J Solids Struct 1995;32(13):1873–92.
[23] Su C, Qin Z, Fan X, Xu Z. Stochastic spline fictitious boundary element method for random vibration analysis of plane elastic problems with structural uncertainties. Probab Eng Mech 2017;49:22–31.
[24] Kamiński M. Iterative scheme in determination of the probabilistic moments of the structural response in the Stochastic perturbation-based Boundary Element Method. Comput Struct 2015;151:86–95.
[25] Venini P, Mariani C. Free vibrations of uncertain composite plates via stochastic Rayleigh-Ritz approach. Comput Struct 1997;64(1–4):407–23.
[26] Zhang Z, Tian J, Huang X, Hua H. Stochastic response analysis of a built-up vibro-acoustic system with parameter uncertainties. Int J Appl Mech 10 (8).
[27] Xiang P, Xia Q, Jiang LZ, Peng L, Yan JW, Liu X. Free vibration analysis of FG-CNTRC conical shell panels using the kernel particle Ritz element-free method. Compos Struct 2021;255(August 2020):112987. https://doi.org/10.1016/j.compstruct.2020.112987.
[28] Sepahvand K, Marburg S, Hardtke HJ. Stochastic free vibration of orthotropic plates using generalized polynomial chaos expansion. J Sound Vib 2012;331 (1):167–79.
[29] da Silva CR, Beck AT. Bending of stochastic Kirchhoff plates on Winkler foundations via the Galerkin method and the Askey-Wiener scheme. Probab Eng Mech 2010;25(2):172–82.
[30] Gupta A, Arun CO. Stochastic meshfree method for elastic buckling analysis of columns. Comput Struct 2018;194:32–47.
[31] Huang W, Huang Q, Liu Y, Yang J, Hu H, Trochu F, Causse P. A Fourier based reduced model for wrinkling analysis of circular membranes. Comput Methods Appl Mech Eng 2019;345:1114–37.
[32] Huang Q, Xu R, Liu Y, Hu H, Giunta G, Belouettar S, Potier-Ferry M. A two-dimensional Fourier-series finite element for wrinkling analysis of thin films on compliant substrates. Thin-Wall Struct 2017;114:144–53.
[33] Huang Q, Liu Y, Hu H, Shao Q, Yu K, Giunta G, Belouettar S, Potier-Ferry M. A Fourier-related double scale analysis on the instability phenomena of sandwich plates. Comput Methods Appl Mech Eng 2017;318:270–95.
[34] Banerjee JR, Ananthapuvirajah A, Liu X, Sun C. Coupled axial-bending dynamic stiffness matrix and its applications for a Timoshenko beam with mass and elastic axes eccentricity. Thin-Wall Struct 2020:107197. https://doi.org/10.1016/j.tws.2020.107197.
[35] Adhikari S, Karličić D, Liu X. Dynamic stiffness of nonlocal damped nano-beams on elastic foundation. Eur J Mech A/Solids 2020;86(June). https://doi.org/10.1016/j.euromechsol.2020.104144.
[36] Kolarevic N, Nefovska-Danilovic M, Petronijevic M. Dynamic stiffness elements for free vibration analysis of rectangular Mindlin plate assemblies. J Sound Vib 2015;359:84–106.
[37] Liu X, Banerjee JR. Free vibration analysis for plates with arbitrary boundary conditions using a novel spectral-dynamic stiffness method. Comput Struct 2016;164:108–26.
[38] Banerjee JR, Papkov SO, Liu X, Kennedy D. Dynamic stiffness matrix of a rectangular plate for the general case. J Sound Vib 2015;342:177–99.
[39] Casimir JB, Kevorkian S, Vinh T. The dynamic stiffness matrix of two-dimensional elements: application to Kirchhoff's plate continuous elements. J Sound Vib 2005;287(3):571–89.
[40] Liu X, Liu X, Zhou W. An analytical spectral stiffness method for buckling of rectangular plates on Winkler foundation subject to general boundary conditions. Appl Math Model 2020;86:36–53. https://doi.org/10.1016/j.apm.2020.05.010.

[41] Liu X, Banerjee JR. An exact spectral-dynamic stiffness method for free flexural vibration analysis of orthotropic composite plate assemblies - Part I: Theory. Compos Struct 2015;132:1274–87.
[42] Liu X, Zhao X, Xie C. Exact free vibration analysis for membrane assemblies with general classical boundary conditions. J Sound Vib 2020;485:115484. https://doi.org/10.1016/j.jsv.2020.115484.
[43] Liu X, Xie C, Dan H-C. Exact free vibration analysis for plate built-up structures under comprehensive combinations of boundary conditions. Shock Vib 2020:5305692. https://doi.org/10.1155/2020/5305692.
[44] Liu X, Li Y, Lin Y, Banerjee J. Spectral dynamic stiffness theory for free vibration analysis of plate structures stiffened by beams with arbitrary cross-sections. Thin-Wall Struct.
[45] Liu X, Sun C, Banerjee J, Dan H-C, Chang L. An exact dynamic stiffness method for multibody systems consisting of beams and rigid-bodies. Mech Syst Signal Process 2021;150:107264. https://doi.org/10.1016/j.ymssp.2020.107264.
[46] Liu X, Liu X, Xie S. A highly accurate analytical spectral flexibility formulation for buckling and wrinkling of orthotropic rectangular plates. Int J Mech Sci 2020;168:105311. https://doi.org/10.1016/j.ijmecsci.2019.105311.
[47] Li K, Gao W, Wu D, Song C, Chen T. Spectral stochastic isogeometric analysis of linear elasticity. Comput Methods Appl Mech Eng 2018;332:157–90.
[48] Li K, Wu D, Gao W, Song C. Spectral stochastic isogeometric analysis of free vibration. Comput Methods Appl Mech Eng 2019;350:1–27.
[49] Adhikari S. Doubly spectral stochastic finite-element method for linear structural dynamics. J Aerosp Eng 2011;24(3):264–76.
[50] Ghanem R, Spanos P. Stochastic finite elements: a spectral approach. New York, USA: Springer-Verlag; 1991.
[51] Sudret B, Der-Kiureghian A. Stochastic finite element methods and reliability, Tech. Rep. UCB/SEMM-2000/08, Department of Civil & Environmental Engineering, University Of California, Berkeley; November 2000.
[52] Scheidt JV, Purkert W. Random eigenvalue problems. New York: North Holland; 1983.
[53] Benaroya H. Random eigenvalues, algebraic methods and structural dynamic models. Appl Math Comput 1992;52:37–66.
[54] Adhikari S. Joint statistics of natural frequencies of stochastic dynamic systems. Comput Mech 2007;40(4):739–52.
[55] Papoulis A, Pillai SU. Probability, random variables and stochastic processes. 4th ed. Boston, USA: McGraw-Hill; 2002.
[56] Scarth C, Cabral SAPH, Silva GHC, Prado AP. Random field simulation over curved surfaces: Applications to computational structural mechanics. Comput Methods Appl Mech Eng 2019;345(3):283–301.
[57] Scarth C, Adhikari S. Modelling spatially varying uncertainty in composite structures using lamination parameters. AIAA J 2017;55(11):3951–65.
[58] Kim H, Shields MD. Modeling strongly non-Gaussian non-stationary stochastic processes using the Iterative Translation Approximation Method and Karhunen-Loève expansion. Comput Struct 2015;161:31–42.
[59] Meirovitch L. Principles and techniques of vibrations. New Jersey: Prentice-Hall International Inc; 1997.
[60] Manohar CS, Adhikari S. Dynamic stiffness of randomly parametered beams. Probab Eng Mech 1998;13(1):39–51.
[61] Manohar CS, Adhikari S. Statistical analysis of vibration energy flow in randomly parametered trusses. J Sound Vib 1998;217(1):43–74.
[62] Adhikari S, Manohar CS. Transient dynamics of stochastically parametered beams. ASCE J Eng Mech 2000;126(11):1131–40.
[63] Gupta S, Manohar CS. Dynamic stiffness method for circular stochastic timoshenko beams. J Sound Vib 2002;253(10):1051–85.
[64] Ghanem R, Sarkar A. Reduced models for the medium-frequency dynamics of stochastic systems. J Acoust Soc Am 2003;113(2):834–46.
[65] Sarkar A, Ghanem R. A substructure approach for the midfrequency vibration of stochastic systems. J Acoust Soc Am 2003;113(4):1922–34. part 1.
[66] Ostoja-Starzewski M, Woods A. Spectral finite elements for vibrating rods and beams with random field properties. J Sound Vib 2003;268(4):779–97.
[67] Machado MR, Adhikari S, Dos-Santos JMC, Arruda JRF. Estimation of beam material random field properties via sensitivity-based model updating using experimental frequency response functions. Mech Syst Signal Process 2018;102(3):180–97.
[68] Zhao H, Rahn CD. Stability of damped membranes and plates with distributed inputs. J Sound Vib 2007;302(3):564–76.
[69] Spanos PD, Beer M, Red-Horse J. Karhunen-Loéve Expansion of Stochastic Processes with a Modified Exponential Covariance Kernel. J Eng Mech 2007;133(7):773–9.
[70] Li J-M, Zhao B, Cheng H, Kardomateas G, Liu L. Nonlinear dynamic response of a sandwich structure with flexible core in thermal environments. J Sandwich Struct Mater 2020:1–36. https://doi.org/10.1177/1099636220930981.
[71] Liu L, Li JM, Kardomateas GA. Nonlinear vibration of a composite plate to harmonic excitation with initial geometric imperfection in thermal environments. Compos Struct 2019;209:401–23. https://doi.org/10.1016/j.compstruct.2018.10.101.
[72] Xie S, Jing K, Zhou H, Liu X. Mechanical properties of Nomex honeycomb sandwich panels under dynamic impact. Compos Struct 2020;235(October 2019):111814. https://doi.org/10.1016/j.compstruct.2019.111814.
[73] Xie S, Wang D, Feng Z, Yang S. Sound absorption performance of microperforated honeycomb metasurface panels with a combination of multiple orifice diameters. Appl Acoust 2020;158:107046. https://doi.org/10.1016/j.apacoust.2019.107046.
[74] Xie S, Yang S, Yang C, Wang D. Sound absorption performance of a filled honeycomb composite structure. Appl Acoust 2020;162:107202. https://doi.org/10.1016/j.apacoust.2019.107202.
[75] Adhikari S, Friswell MI. Random matrix eigenvalue problems in structural dynamics. Int J Numer Meth Eng 2007;69(3):562–91.